Bestrophin-4 relays Hes4 and interacts with Twist1 to suppress epithelial-to-mesenchymal transition in colorectal cancer cells

Zijing Wang[1], Bihan Xia[1], Shaochong Qi[1], Xian Zhang[1], Xiaoshuang Zhang[1], Yan Li[1], Huimin Wang[1], Miao Zhang[2,3], Ziyi Zhao[4], David Kerr[2], Li Yang[1], Shijie Cai[2] * and Jinlin Yang[1]*

1. Department of Gastroenterology and Hepatology, Sichuan University-University of Oxford Huaxi Joint Centre for Gastrointestinal Cancer, West China Hospital, Sichuan University, Chengdu 610000, China
2. Nuffield Division of Clinical Laboratory Sciences, Radcliffe Department of Medicine, University of Oxford, John Radcliffe Hospital, Oxford OX3 9DU, UK
3. College of Acupuncture and Moxibustion, Fujian University of Traditional Chinese Medicine, Fuzhou, 350102, China.
4. TCM Regulating Metabolic Diseases Key Laboratory of Sichuan Province, Hospital of Chengdu University of Traditional Chinese Medicine, Chengdu, 410000, China

***Correspondence:** yangjinlin@wchscu.cn, shijie.cai@ndcls.ox.ac.uk

*Prof. Jinlin Yang

Sichuan University-University of Oxford Huaxi Joint Centre for Gastrointestinal Cancer，Department of Gastroenterology and Hepatology, West China Hospital, Sichuan University

Chengdu 610000, China

Tel: +86-18980602058

21 Fax: +86-28-85423387

22 Email: yangjinlin@wchscu.cn

23

24 *Dr. Shijie Cai

25 Nuffield Division of Clinical Laboratory Sciences, Radcliffe Department of Medicine

26 University of Oxford, John Radcliffe Hospital

27 Oxford OX3 9DU, UK

28 Tel: +44-1865-221110

29 Fax: +44-1865-220980

30 Email: shijie.cai@ndcls.ox.ac.uk

31 **Running Title**: BEST4 deters EMT by downregulating Twist1 expression

32

33

34

35

36

37

38

Abstract: Bestrophin isoform 4 (*BEST4*) is a newly identified subtype of the calcium-activated chloride channel family. Analysis of colonic epithelial cell diversity by single cell RNA-sequencing has revealed the existence of a cluster of *BEST4*+ mature colonocytes in humans. However, if the role of *BEST4* is involved in regulating tumour progression remains largely unknown. In this study, we demonstrate that *BEST4* overexpression attenuates cell proliferation, colony formation, and mobility in colorectal cancer (CRC) *in vitro*, and impedes the tumor growth and the liver metastasis *in vivo*. *BEST4* is coexpressed with hairy/enhancer of split 4 (*Hes4*) in the nucleus of cells, and *Hes4* signals *BEST4* by interacting with the upstream region of the *BEST4* promoter. *BEST4* is epistatic to *Hes4* and downregulates Twist1, thereby inhibiting epithelial-to-mesenchymal transition (EMT) in CRC. Conversely, knockout of BEST4 using CRISPR/Cas9 in CRC cells revitalises tumor growth and induces EMT. Furthermore, the low level of the *BEST4* mRNA is correlated with advanced and the worse prognosis, suggesting that *BEST4* functions as a tumor suppressor in CRC.

Keywords: Colorectal cancer; Bestrophin 4; Hairy/enhancer of split 4; Twist1; Epithelial-mesenchymal transition;

Introduction

Colorectal cancer (CRC) is a common tumour worldwide. A steady increase in the morbidity and mortality of CRC has been reported (Rawla et al., 2019). When diagnosed in advanced stages, epithelial-mesenchymal transition (EMT) may occur as CRC metastasize to distal organs (Pastushenko and Blanpain, 2019; Sunlin Yong, 2021; Yeung and Yang, 2017; Zhang et al., 2021). EMT is a reprogramming process in which epithelial E-cadherin and ZO-1 are suppressed, and mesenchymal N-cadherin and vimentin are induced, transcriptionally mediated by Twist and the Snail family (Dongre and Weinberg, 2019).

The inhibition of EMT in breast cancer and prostate cancer has been associated with calcium-activated chloride channels (CaCCs) (Porretti et al., 2018; Walia et al., 2012), leading to various evaluations of CaCCs as a potential for cancer therapy (Li et al., 2017; Miotto and Struhl, 2006; Qu et al., 2019; Sui et al., 2014). The bestrophin (*BEST*) chloride channel, which is a member of a recently identified gene family, encodes several integral membrane proteins expressed on the basolateral membranes of epithelial cells; they regulate CaCCs to maintain homeostasis (Marmorstein et al., 2009; Tsunenari et al., 2003). Although there are four human evolutionarily-related genes (*BEST1–BEST4*) (Miller et al., 2019; Tsunenari *et al.*, 2003), variant 4 is expressed predominantly in the colon (Fagerberg et al., 2014), where it gates electrolyte transportation in human intestinal epithelial cells (Ito et al., 2013). However, the role of *BEST4* in the development of CRC and the mechanism behind its regulation are currently unknown.

In a recent analysis based on single cell RNA-sequencing analysis, it was discovered that a group of mature colonocytes expresses *BEST4* (Parikh et al., 2019), and the subset of this group coexists with

79 hairy/enhancer of split 4 positive (*Hes4*$^{+}$) cells (Parikh et al., 2019). *Hes4* belongs to a family of seven
80 Hes genes (*Hes1–7*) that encodes a transcription factor with a basic helix-loop-helix motif. It is known
81 to play a critical role in determining the fate and differentiation of progenitor cells during the
82 development of various organs. Inhibiting the Twist1 transcriptional factor has been shown to mediate
83 commitment to the differentiation of human bone marrow stem cells, as reported by several studies (El
84 Yakoubi et al., 2012; Murato and Hashimoto, 2009; Nichane et al., 2008; Cakouros et al., 2015). Given
85 this information, it is tempting to speculate that BEST4 may be associated with Hes4 and Twist1 in
86 regulating EMT during CRC progression.

87 The aims of the present study are to: (1) establish the role *BEST4* in CRC growth *in vitro* and *in*
88 *vivo*; (2) determine the underlying molecular mechanisms by which *BEST4* interacts with Hes4 and
89 Twist1, and regulates EMT; and (3) explore the correlation of *BEST4* gene expression with prognosis of
90 CRC.

91

92

93

94

95

96

97

98

99

100 ## Results

101 ***BEST4* inhibits CRC proliferation, clonogenesis, migration, and invasion *in vitro***

102 To evaluate the effect of BEST4 on tumour growth, we constructed *BEST4*-expressing HCT116 and
103 Caco2 CRC cell lines (**Figure 1-supplemental figure 1A-1C)** and showed that *BEST4* overexpression
104 halved cell proliferating rates of their respective empty vector (EV) controls when they were monitored
105 in live and analysed using InCucyte (**Figures 1A and 1B**). This was accompanied by decreased cell
106 viability (**Figure 1-supplemental figure 1D and 1E)**. To determine the causal role of BEST4 in CRC
107 tumorigenesis, we knocked out the *BEST4* gene in HCT-15 using a CRISPR/Cas9 system (**Figure 1-**
108 **supplemental figure 1F-H**). Consequently, there was a 50% increase in proliferation rates and viability
109 compared with the parental control (**Figures 1C and 1D; Figure 1-supplemental figure 1I**). Rescued
110 expression of BEST4 was able to reverse the observed effects on HCT-15 (**Figure 1D; Figure 1-**
111 **supplemental figure 1I**).

112 In contrast to the controls, BEST4 overexpression decreased colony formations of HCT116 and
113 Caco2 by 60% and 70%, respectively (**Figure 1E**). While BEST4 deletion increased the number of
114 colonies by five-fold in HCT-15 (**Figure 1F**), the rescued expression counteracted its enhancement
115 (**Figure 1F**).

116 Furthermore, overexpression of *BEST4* in HCT116 inhibited transwell migration and invasion by
117 70% and 80%, respectively, compared to EV controls (**Figure 1G**). But *BEST4* ablation in HCT-15
118 increased cell migration and invasion by two-fold and three-fold, respectively. These pro-tumor effects
119 on HCT-15 were also reversible when BEST4 expression was rescued (**Figure 1H**).

120 Collectively, these findings suggest the tumour-suppressive role of *BEST4* in CRC growth *in vitro*.

121 ***BEST4* deters EMT in CRC *in vitro* and *in vivo***

122 Because EMT initiation is a critical process in tumour progression (Acloque et al., 2009), we
123 evaluated the effect of *BEST4* on EMT using qPCR and found that *BEST4* expression upregulated *CDH1*
124 and *ZO-1* and downregulated *vimentin* and *Twist1* in HCT116 compared with the control ($p < 0.05$)
125 (**Figures 2A**). Conversely, knockout of *BEST4* in HCT15 downregulated *CDH1* and *ZO-1* and
126 upregulated *vimentin* and *Twist1*. Rescued expression of BEST4 in HCT-15 reversed these gene
127 alterations (**Figures 2B**). Changes of these genes were consistent with their corresponding protein
128 expression as analysed by immunoblotting (**Figures 2C and 2D**).

129 Next, we subcutaneously implanted *BEST4*-HA-expressing HCT116 and EV control cell lines into
130 BALB/c nude mice and monitored tumour growth weekly. When they reached the maximum allowable
131 volumes (day 32), the animals were culled, and tumours were harvested. Essentially, the sizes and
132 weights of tumours in *BEST4* overexpression group were only half of the EV control (**Figures 2E and**
133 **2F**), in conjunction with the similar magnitude reduction of Ki67+ cells as analyzed by
134 immunohistochemistry (**Figure 2G and 2H**). Further analysis of the HCT116 tumour tissue lysates
135 showed that *BEST4* deterred EMT by upregulating E-cadherin and, downregulating vimentin and Twist1
136 (**Figures 2I and 2J**).

137 We also evaluated the inhibitory role of BEST4 in a model of CRC to the liver metastasis by
138 intrasplenically injecting HCT-15 cell lines with BEST4 knockout (BEST4gRNA) or the wild-type
139 control (gRNA) or the knockout with the rescue (BEST4-Rescued) into BALB/c nude mice. We observed
140 that there were 2-fold greater of the liver metastatic nodules in the BEST4 deficient tumors than the
141 control (**Fig. 2K and 2L**). Conversely, the reconstituted BEST4 expression had no visible metastatic
142 nodules in the liver, and the pathological analysis of the tissue sections by H&E staining also confirmed
143 no detectable metastatic loci in the tissue sections (**Fig. 2K and 2L**).

144

145 These findings indicate the role of BEST4 in suppressing CRC tumorigenic activities, through
146 counteracting EMT induction in models of *in vitro* and *in vivo*.

147 **Hes4 upstream regulation of BEST4**

148 Given the co-expression of *BEST4*$^{+}$ and *Hes4*$^{+}$ in a human colonic epithelial lineage (Parikh *et al.*,
149 2019), we sought to investigate their biological interactions during tumour growth. Upon transfecting the
150 Flag-*Hes4* plasmid DNA into HCT116, we observed a responsive upregulation of both endogenous
151 *BEST4* mRNA and protein levels compared to the control transfectant (**Figure 3A; Figure 3-**
152 **supplemental figure 1A)**. This intrinsic association was further supported by knocking down the
153 endogenous Hes4 with two pairs of shRNAs in LST174 that resulted in downregulation of endogenous
154 BEST4 (**Figure 3B; Figure 3-supplemental figure 1B**).

155 To explore how Hes4 regulates *BEST4* expression at the transcriptional level, we transfected a
156 *BEST4* promoter-driven luciferase DNA construct into *Hes4*-expressing HCT116 and assessed the
157 promoter activity using a dual-luciferase assay. Our results showed a four-fold increase in the promoter
158 activity compared to the EV control (**Figure 3C**), Furthermore, ChIP-qPCR analysis using a Flag
159 antibody to IP for Hes4 revealed a twelve-fold enrichment of the P3 region upstream of the *BEST4*
160 transcriptional start site compared to the control (**Figure 3D**). Interestingly, *BEST4* overexpression in
161 HCT116 cells did not affect *Hes4* mRNA expression as quantified by qPCR (**Figure 3-supplemental**
162 **figure 1C**), suggesting that *Hes4* regulates *BEST4* expression upstream. This speculation is supported by
163 immunofluorescence staining, where we observed nuclear co-localization of BEST4 (green) and Hes4

164 (red) in HCT116 cells co-transfected with *BEST4*-HA and Flag-*Hes4* plasmid DNAs, along with
165 additional cytoplasmic expression of *BEST4* (**Figure 3E)**.
166 To evaluate the association of *BEST4* with Hes4 at the translational level, we co-transfected their
167 HA-tagged *BEST4* and Flag-*Hes4* plasmid DNAs into HEK293 cells, along with the respective single
168 transfectant control. By conducting IP with antibodies specific to Flag or HA, we showed that *BEST4*
169 and *Hes4* were reciprocally copurified from the nuclear protein lysates, but not with IgG controls (**Figure**
170 **3F**).
171 Collectively, these findings indicate that *BEST4* interacts with *Hes4* at both transcriptional and
172 translational levels.

173 ***BEST4* relays *Hes4* signal and directly downregulates Twist1 leading to EMT inhibition**
174 **independent of the channel function in CRC**

175 Because a step of *Hes4* in committing to human bone marrow stromal/stem cell lineage-specific
176 development is mediated by Twist1 downregulation (Cakouros *et al.*, 2015), with evidence of direct
177 interaction between BEST4 and Hes4 observed in HCT116, it is plausible that they could exploit Twist1
178 to regulate EMT. To test this notion, we transfected a Twist1 promoter-driven luciferase DNA construct
179 into HCT116. In comparison with the EV control, Flag-*Hes4* or *BEST4*-HA transfectants significantly
180 decreased Twist1 promoter activity by almost half, as evaluated by the dual-luciferase assay (**Figure 4A)**.
181 Essentially, the *BEST4* transfectant enhanced inhibition of the Twist promoter by 70% in *Hes4*-
182 expressing HCT116 **(Figure 4B),** hence suggesting that *BEST4* mediates the inhibition of the Twist1
183 promoter activity by *Hes4*. This effect was also observed when endogenous Hes4 was knocked down

184 using shRNAs in HCT116 cells transfected with *BEST4*-HA plasmid DNA (**Figure 4C**).

185 The association of BEST4 with the Twist1 promoter activity was also evidenced by their nuclear
186 colocalization after transfecting BEST4-HA and Myc-Twist1 plasmid DNAs into HCT116 (**Figure 4-**
187 **supplemental figure 1A)**. Co-IP with antibodies to Myc or HA showed that they were copurified from
188 the nuclear protein lysates, but not with the IgG controls from the transfectant cell lysates (**Figure 4D；**
189 **Figure 4-supplemental figure 1A**). Additionally, the knockdown of endogenous *BEST4* in Hes4-
190 expressing HCT116 cells substantially decreased Flag-Hes4 coprecipitation from the nuclear protein
191 lysates, while Myc-Twist1 expression remained constant, as determined by co-IP with antibodies to Flag
192 or My (**Figure 4E；Figure 4-supplemental figure 1B**).

193 We then investigated the impact of Hes4 expression on EMT induction by overexpressing Hes4 in
194 HCT116 cells. Our results showed there were upregulation of ZO-1 and E-cadherin epithelial molecules,
195 and downregulation of Twist1 protein (**Figure 4F)** and the *vimentin* mRNA **(Figure 4-supplemental**
196 **figure 1C)**. The vimentin protein appeared to be undetectable in HCT116, which was consistent with a
197 previous report (Roger et al., 2010). Nevertheless**,** knocking down endogenous *Hes4* in LS174T cells
198 using shRNAs targeting two *Hes4* domains caused the opposite effect **(Figure 4G).**

199 To determine if BEST4 is downstream signal that relays Hes4 to regulate Twist1 expression and
200 consequently EMT induction, we knocked down endogenous *BEST4* with siRNAs in Hes4-expressing
201 HCT116 and showed the corresponding downregulation of E-cadherin and ZO-1, with upregulation of
202 Twist1 protein and the *vimentin* mRNA, as analyzed by immunoblotting and qPCR **(Figure 4H; Figure**
203 **4-supplemental figure 1D**). The opposite was true when BEST4 was overexpressed in LS174T **(Figure**

204 **4I**). Therefore, these findings infer *BEST4*-mediated upstream *Hes4* to directly downregulate Twist1 and
205 subsequently deter EMT in CRC.

206 Given the physiological role of *BEST4* plays in regulating chloride/calcium flux, we evaluated the
207 channel functional effect on EMT induction. After respectively incubating *BEST4*-expresing HCT116
208 and the EV control with 300μM DIDS (a broad blocker of chloride channel), or a gradient increase in
209 doses of CaCCinh-A01 (a specific inhibitor of native calcium-activated chloride channels), or 1μM
210 ionomycin (a calcium ionophore to activate the chloride channel) as published previously (Liu *et al*, 2015;
211 Uwada *et al,* 2019), we showed that *BEST4* significantly increased chloride/calcium fluxes and activated
212 their exchanges and the expected inhibition by DIDS, CaCCinh-A01 or ionomycin (**Fig. 4-**
213 **supplementary figure 5A-5C**). Through immunoblotting analysis, we recapitulated that *BEST4*
214 simultaneously upregulated both ZO-1 and E-cadherin, and downregulated Twist1. Essentially, the levels
215 of these proteins remained constantly expressed when the cells were treated with DIDS or CaCCinh-A01
216 or ionomycin, respectively (**Fig. 4-supplementary figure 5D-5F**). Hence, these results suggest *BEST4*
217 protein-mediated EMT suppression is independent of its channel function in HCT116.

218 **Correlation of the *BEST4* gene with clinicopathology and outcomes of patients diagnosed with**
219 **CRC**

220 We showed evidence of the endogenous *BEST4* mRNA and protein expression in HCT116 and
221 LS174T CRC cell lines (**Figures 3A and 3B**); these findings prompted us to explore the potential
222 clinically significant *BEST4* expression in CRC. Initially with high-throughput whole transcriptome
223 sequencing analysis of five pairs of CRCs and adjacent normal tissues (ANTs), we identified several
224 significantly downregulated genes in CRC compared to ANTs; *BEST4* was in the top four **(Figures 5A**

225 **and 5B)**. Further validation by qPCR in the paired tissues of 50 colorectal adenomas and 124 CRC
226 showed that the *BEST4* gene was expressed significantly less in adenomas and tumours than in ANTs
227 **(Figures 5C and 5D)**. Immunoblotting analysis of tissue lysates from five paired randomly selected
228 samples showed that BEST4 protein was downregulated in CRC (**Figures 5E**). Using public datasets of
229 The Cancer Genome Atlas (TCGA) and the Genotype-Tissue Expression (GTEx), we measured *BEST4*
230 gene expression in CRC and matched normal tissues with the online Gene Expression Profiling
231 Interactive Analysis (GEPIA) tool (http://gepia.cancer-pku.cn/). As shown in **Figure 6-supplemental**
232 **figure 1A,** the normal colorectal control tissues consistently expressed higher *BEST4* than the CRC.

233 We further evaluated the clinicopathological significance of *BEST4* expression in CRC patients by
234 examining its correlation with gender, tumour-node-metastases stage, and lymph node metastasis based
235 on the eighth edition of the American Joint Committee on Cancer Staging Manual (M. B. Amin et al.,
236 Springer, 2017). Interestingly, *BEST4* expression in males was twice as high as in females (p=0.022,
237 **Table 1**). Accordingly, high *BEST4* gene expression correlated with more advanced stages (p=0.02,
238 **Table 1**) and lymph node metastasis (between 0 and 2) (p=0.032, **Table 1**). Patients with high *BEST4*
239 expression had better overall survival than those with low expression (p<0.01, **Figure 5F**), which was
240 confirmed by univariate survival analysis showing a lower risk of death (p<0.001, **Table 2**). Multivariate
241 Cox regression analysis indicated that low levels of BEST4 mRNA were associated with poor prognosis
242 of CRC patients (Hazard Ratio [HR], 0.285; 95% confidence interval, 0.157–0.606; P<0.001; **Table 2**).

243 After the significant reduction of the *Hes4* gene through RNA sequencing analysis of our CRC
244 patients (**Figure 6-supplemental figure 1B and 1C**), we proceeded to investigate the connection
245 between *BEST4* and *Hes4* genes in TCGA and GTEx (http://gepia.cancer-pku.cn/). Our findings revealed

246 a positive correlation between these genes (R = 0.47, $p<0.001$) (**Figure 6-supplemental figure 1D**),
247 providing further evidence of their association in CRC. Furthermore, we conducted additional mining of
248 TCGA or GTEx datasets using the GEPIA tool (http://gepia.cancer-pku.cn/) and observed a positive
249 correlation between *BEST4* and the *CDH1* mRNA (R = 0.77, $p<0.001$), with a negative correlation with
250 *vimentin* (R =–0.49, $p<0.001$) and *Twist* mRNA (R =–0.39, $p<0.001$)) (**Figure 6-supplemental figure**
251 **1E-G**). These correlation analyses of RNA sequencing data from our patients and publicly available
252 datasets underscore the association of low *BEST4* expression with worse outcomes in malignant CRC.
253
254
255
256
257
258
259
260
261
262
263
264
265
266

267 **Discussion**

268 In cancer cell cultures and mouse tumour xenografts, the present study shows that *BEST4* inhibits
269 the development of CRC. An axis comprising *Hes4/BEST4*/Twist1 governs the induction of EMT in
270 CRC. *BEST4* interacts with *Hes4* at the transcriptional and translational levels, and directly
271 downregulates Twist1 expression, resulting in EMT inhibition but independent of its channel functions.
272 Our findings support the notion in several ways: (1) *Hes4* binds to the promoter region of *BEST4*; (2)
273 *BEST4* colocalizes with *Hes4* and Twist1 in the nucleus of cells, and protein-protein interactions; (3) the
274 *BEST4* inhibitory role in EMT exhibits upregulation of epithelial ZO-1 and E-cadherin, and
275 downregulation of mesenchymal vimentin and Twist1 in CRC; and finally (4) low *BEST4* mRNA levels
276 were significantly correlated with malignant lesions and worse outcomes of CRC patients. To the best of
277 our knowledge, this is the first characterization of the role of *BEST4* in suppressing CRC progression
278 and the underlying molecular mechanisms.

279 CaCCs are expressed widely in several types of epithelial and endothelial cells and are classified as
280 calcium-dependent chloride channels (e.g., anoctamin-1 [ANO1 or TMEM16]), chloride channel
281 accessory proteins (CLCAs), and members of the BEST family. The latter is a recent addition to the class
282 of molecularly defined chloride channels (Huang et al., 2012). Calcium-dependent chloride channels and
283 CLCAs are differentially expressed in CRC and normal colon tissues, exerting pro- or anti-growth effects,
284 while little is known of BEST family in CRC (Li *et al.*, 2017; Sanders et al., 2012; Sui *et al.*, 2014; Yang
285 et al., 2015). There are four subtypes of the *BEST* family in mammals that assemble as pentamers to form
286 Ca^{2+}-activated Cl^- channels and maintain cellular physiological functions (Marmorstein *et al.*, 2009;

287 Milenkovic et al., 2008; Tsunenari *et al.*, 2003). Subtypes of *BEST1-3* are responsible for vitelliform
288 macular dystrophy, regulating the cilia of olfactory sensory neuronal activity; others regulate cGMP-
289 dependent calcium-activated chloride conductance in vascular smooth muscle cells (Matchkov et al.,
290 2008; Pifferi et al., 2009). An intrinsic function of the *BEST4* gene in modulating CRC growth remains
291 poorly illustrated. In the present study, we demonstrated that *BEST4* functionally inhibits the
292 development of CRC *in vitro* and *in vivo*. *BEST4* is transcriptionally regulated and physically interacts
293 with upstream *Hes4*, leading to downregulation of Twist1 and EMT suppression. This suppression is
294 independent of physiological Ca^{2+}-activated Cl^- channels since inhibition of BEST4-associated Ca^{2+}-
295 and Cl^- fluxes did not alter ZO-1/E-Cadherin and Twist1 protein expression.

296 The recent identification of a heterogeneous *BEST4*$^+$ and *Hes4*$^+$ subgroup in a human colonic
297 epithelial lineage (Parikh *et al.*, 2019) led us to consider their potential role in regulating CRC
298 progression. Among the Hes family, which is associated with intestinal progenitor cells in adenoma
299 transformation, *Hes1* and *Hes4* are a paralog pair, with other members more distantly related (Katoh and
300 Katoh, 2004). While *Hes1* has been reported to induce EMT and promote metastasis and chemoresistance
301 in CRC (Sun et al., 2017; van Es et al., 2005; Yuan et al., 2015), *Hes4* is identified by our present study
302 capable of combating EMT induction in a *BEST4*-dependent manner that is regulated at both
303 transcriptional and translational levels.

304 The Twist1 transcriptional factor plays a crucial role in inducing EMT, which contributes to the
305 malignant lesions (Yang et al., 2004). Its physical interaction with *Hes4* determines human bone marrow
306 stromal/stem cell differentiation (Cakouros *et al.*, 2015). Twist1, a basic helix-loop-helix transcription

307 factor, represses the expression of E-cadherin and ZO-1 and induces several mesenchymal markers
308 including vimentin, which is a pivotal predictor of CRC progression (Nagai et al., 2016; Yang *et al.*,
309 2004; Bulzico et al., 2019; Meng et al., 2018; Nagai *et al.*, 2016; Yang *et al.*, 2004; Vesuna et al., 2008;
310 Yang *et al.*, 2004; Yusup et al., 2017; Zhu et al., 2015). Despite Twist1 importance in CRC, little is
311 known about how it is controlled during EMT induction. Our present study reveals that Twist1
312 colocalized and interacted with *BEST4* in the nucleus of CRC HCT116 cells, leading to downregulation
313 of Twist1 and inhibition of EMT. *Hes4* also caused the same effect, but through intermediation with
314 *BEST4*. Although the mechanistic insights of their interplay remain to be elucidated, the present study
315 identifies the *Hes4-BEST4-Twist1* axis that contributes to counter EMT in the development of CRC
316 **(Figure 5G)**.

317 Lastly, our analysis of correlations reveals the clinical significance of *BEST4* expression in CRC.
318 In particular, the mRNA levels of *BEST4* were lower in tissues of both precancerous adenomatous lesions
319 and CRC than ANTs. These alterations are significantly correlated with large tumour size, positive nodes,
320 and poor overall survival, especially in male patients. Interestingly, a previous study conducted on a
321 Chinese cohort reported an approximately 40% higher incidence of CRC in males than in females (Zhang
322 et al., 2019). But it remains to be investigated whether sex hormone-related factors plays a role in the
323 gender-specific downregulation of *BEST4* and its impact on CRC in males (Yu et al., 2020).

324 In conclusion, the functional significance of *BEST4* in CRC development and its interplay with
325 other molecules is completely unknown. The present study demonstrates the role of *BEST4* in inhibiting
326 CRC proliferation, migration, and invasion both in models of in vitro and in vivo. Mechanically, *BEST4*
327 is epistatic to *Hes4* for downregulating Twist1 and inhibits EMT in CRC. Therefore, we reveals a

328 previously unknown mechanism of the *Hes4-BEST4-Twist* axis that restrains the progression of CRC.

329

330

331

332

333

334

335

336

337

338

339

340

341

342

343

344

345

346

347

348

349 **Materials and Method**

350 **Clinical samples**

351 A total of 124 samples of paired CRC and adjacent normal tissue and 50 samples of paired adenoma
352 and ANT were collected randomly from clinical specimens from patients undergoing intestinal resections
353 or upper gastrointestinal endoscopies at the Department of Gastrointestinal Surgery and Digestive
354 Endoscopy Centre, West China Hospital, China, between January and December 2013. All patients were
355 followed until December 2018 or until death. Samples from patients with malignant tumours in other
356 organs, from patients who received preoperative chemotherapy or radiotherapy, and from patients with
357 incomplete follow-up data were excluded. The survival time was calculated from the surgery date to the
358 follow-up deadline (above) or until the date of death. The Ethics Committee of West China Hospital,
359 Sichuan University (Sichuan, China) approved the study. All procedures were performed per the 1964
360 Declaration of Helsinki. Written informed consent was obtained from all participants.

361 **Cell cultures and reagents**

362 The human colon cancer cell lines Caco-2, HCT116, HCT-15, and LS174T were purchased from
363 The American Type Culture Collection (Manassas, VA, USA). Cells were authenticated using short
364 tandem repeat analysis performed within two years of receipt. Cells at passages >15 were not used. All
365 cells were maintained in Dulbecco's Modified Eagle's medium (DMEM; Gibco, Waltham, MA, USA)
366 supplemented with 10% foetal bovine serum (FBS), 100 U/mL penicillin, and 100 mg/mL streptomycin.
367 Before each experiment, cells were provided with low glucose (1 g/L) DMEM with 5% FBS before
368 adding experimental reagents. All cell lines were frequently examined using the MycoAlert™

369 Mycoplasma Detection Kit (Lonza, Verviers, Belgium) to ensure they remained free of mycoplasma
370 contamination.

371 **Tumour and CRC hepatic metastasis mouse xenografts**

372 Four-week-old female BALB/c nude mice were housed under standard conditions. The mice were
373 randomized into two groups, with eight mice per group. HCT116 cells (5×10^6 cells in 0.1 mL phosphate-
374 buffered saline) transduced with the lentivirus containing *BEST4* or EV were injected subcutaneously
375 into the right dorsal flank of mice. Tumour growth was measured twice a week using callipers, and
376 tumour volumes were calculated as length x width^2 x 0.5. Mice were sacrificed at 32 days, and tumour
377 weight was measured at the end of the experiment. For further analysis, the excised tumour tissues were
378 divided into two parts and embedded in paraffin or preserved at −80 °C for further analysis.
379 For the liver metastasis of CRC, intrasplenic injections of HCT-15 cells with BEST4-knockout
380 (BEST4-gRNA), BEST4-rescued or control (EV-gRNA) (5×10^6 cells in 0.1 mL PBS) were performed
381 into 6-week-old Balb/c nude mice as described previously[2]. There were 3 mice/group. Briefly, at day 28
382 after the procedure, mouse livers were paraffin embedded and the sections for H&E staining. The
383 numbers of the metastatic nodules on the livers were double-blind visually quantified and confirmed by
384 a pathologist.
385 The Animal Ethics Committee approved animal experiments of West China Hospital, Sichuan
386 University (Sichuan, China).

387 **CRC cell lines with overexpression of *BEST4***

388 Forced overexpression of *BEST4* was examined in HCT116 and Caco2 CRC cells in which the
389 C-terminal HA epitope-tagged human *BEST4* gene with GFP (*BEST4*-HA-GFP) or GFP alone was
390 introduced by lentivirus-mediated gene transfer. Fluorescence-activated cell sorting (FACS) was
391 performed to obtain single cells distributed into 96-well plates. Three independent lines with the highest
392 levels of BEST4 expression were used for subsequent experiments (**Figures S1A and S1B**). *BEST4*
393 mRNA and HA-tagged protein levels were significantly higher in HCT116 and Caco2 cells transfected
394 with *BEST4*-HA plasmids than those transfected with the empty vector (EV) alone (**Figure S1C**). The
395 *BEST4*-overexpressing cell lines were named "HCT116 *BEST4*-HA" and "Caco2 *BEST4*-HA." Cells
396 transfected with the EV alone were referred to as "HCT116 EV" and "Caco2 EV."

397 **CRISPR/Cas9-mediated knockout of *BEST4***

398 *BEST4*-depleted HCT-15 cells were generated with CRISPR/Cas9 gene-editing technology using a
399 dual sgRNA approach. Two sequences that targeted exon 3 within the *BEST4* active fragment (5'-
400 TGACTCTCGTGGTGAACCGC-3' and 5'-CCGAGATGACGCACATCAGC -3') were inserted into
401 the pU6-gRNA-Cas9-EGFP vector (GenePharma, Shanghai, China) to generate a CRISPR/Cas9 *BEST4*
402 knockout plasmid. Excision of the targeted 44 bp genomic fragment resulted in splicing errors in exons
403 2 to 4 and generated a premature STOP codon that abrogated functional gene expression (**Figures S1F**
404 **and S1G**). Cells were transfected with these plasmids, and GFP^+ cells were FACS-sorted as single cells
405 into 96-well plates. After culturing for three weeks, cells were distributed into two 24-well plates, and
406 the appropriate deletion was verified by sequencing. Only cell lines with homozygous deletions were
407 used. Three independent lines generated using this method were used for subsequent experiments and

408 were named "HCT15 *BEST4*-gRNA." Diminished expression of immunoreactive BEST4 protein was
409 confirmed by immunoblotting (**Figure S1H**). The same overexpression strategy was adopted to rescue
410 BEST4 expression in *BEST4* knockout HCT-15 cells, named "HCT15 *BEST4*-Rescued."

411 **Plasmids and transfection/transduction**

412 Expression plasmids encoding *BEST4* (GeneID: 266675, NM_153274; vector: pCDH-CMV-MCS-
413 EF1-CopGFP-T2A-Puro) containing a C-terminal hemagglutinin (HA) epitope tag, *HES4* (GeneID:
414 57801, NM_001142467.2; vector: pCDH-CMV-MCS-EF1- CopGFP-T2A-Puro) containing a N-
415 terminal Flag epitope tag,were synthesized by Public Protein/Plasmid Library (Nanjing, China).
416 According to the manufacturer's instructions, Lipofectamine 3000 (Invitrogen, Carlsbad, CA, USA) was
417 used in cell transfection experiments.

418 To generate a model of CRC with forced overexpression of *Hes4*, cells were transfected with
419 lentiviral pCDH-CMV-MCS-EF1-CopGFP-T2A-Puro vectors containing human Hes4 cDNA and
420 selected with puromycin (Invivogen, San Diego, CA, USA) at 10 μg/mL introduced 48 h after
421 transfection.

422 For short hairpin RNA (shRNA) and RNA silencing (siRNA) experiments, HEK293 cells were co-
423 transduced with lentiviral vectors carrying shRNA targeting *HES4* (Public Protein/Plasmid Library,
424 Nanjing, China; target sequences are listed in **Table S1**). Supernatants were collected at 48 and 72 h for
425 analysis. Scrambled shRNAs were used to control for non-specific effects. Transduction was performed
426 by mixing aliquots of lentivirus with a standard medium containing 10 μg/mL puromycin (Invivogen) to
427 remove untransduced cells. GeneSolution siRNAs targeting *BEST4* (*BEST4*-siRNA) were used to silence

428 gene expression. Scrambled siRNA (SCR) was used as a control (Qiagen, Hilden, Germany). The target
429 sequences of the *BEST4* siRNAs are listed in **Table S1**. For siRNA experiments, cells were seeded one
430 day before transfection in an antibiotic-free medium and grown to 60% confluency in six-well plates.
431 Cells were transfected using Lipofectamine 3000 as per the manufacturer's protocol. The efficiency of
432 RNA interference was determined using quantitative polymerase chain reaction (qPCR) and western
433 blotting.

434 **RNA isolation, cDNA library preparation, sequencing, and data analysis**

435 Total RNA was isolated using a High Pure RNA Isolation Kit (Roche, Basel, Switzerland). RNA
436 samples with an RNA integrity number (RIN) ≥7.0 and a 28S:18S ratio ≥ 1.5 were used in subsequent
437 experiments. Sequencing libraries were generated and sequenced by CapitalBio Technology (Beijing,
438 China). A total amount of 3 μg RNA per sample was used. Briefly, the Ribo-Zero™ Magnetic Kit
439 (Epicentre) was used to remove rRNA from the total RNA, and then the NEBNext Ultra RNA Library
440 Prep Kit for Illumina (NEB, USA) was used to construct the libraries for sequencing following the
441 manufacturer's instructions. The RNA was fragmented into pieces of ~200 base pairs in length in
442 NEBNext First-Strand Synthesis Reaction Buffer (5X). The first-strand cDNA was synthesized from the
443 RNA fragments using reverse transcriptase and random hexamer primers, and then the second-strand
444 cDNA was synthesized in Second-Strand Synthesis Reaction Buffer with dUTP Mix (10x). The end of
445 the cDNA fragment was subjected to an end-repair process that included the addition of a single "A"
446 base followed by ligation of the adapters. Products were purified and enriched using PCR to amplify the
447 library DNA. The final libraries were qualified using Agilent 2100 and quantified using the KAPA
448 Library Quantification Kit (KAPA Biosystems, South Africa). Finally, the libraries were subjected to

449 paired-end sequencing with a paired-end 150-base pair reading length on an Illumina NovaSeq sequencer
450 (Illumina).
451 The sequencing quality of raw data in *fastq* format was assessed using FastQC, and then low-quality
452 data were filtered using the Next Generation Sequencing Quality Control platform. The high-quality
453 clean reads were then aligned to the reference genome using Tophat2 with default parameters. The
454 genome of the human genome version of hg38 (UCSC) was used as the reference. Cufflinks and
455 Cuffmerge software packages were used to assemble the transcripts. All subsequent comparative
456 analyses of lncRNAs and mRNAs were based on the results of the transcripts. Transcripts corresponding
457 to mRNAs or lncRNAs were collected from databases and treated as known lncRNAs and annotated
458 based on information from public databases. The transcripts were treated as novel lncRNAs when their
459 sequence length was >200 and when they were predicted to be non-coding RNAs. Differential expression
460 analyses were performed using the limma package and edgeR. Functional annotation and enrichment
461 analyses were performed using KOBAS 3.0. The target genes of the mRNAs were predicted based on
462 cis- and trans-patterns based on the location on the reference genome and sequence similarity. The raw
463 sequence data reported in this paper were deposited in the NCBI Sequence Read Archive with accession
464 number PRJNA690126.

465 **RNA extraction and real-time PCR**

466 Total RNA was isolated from cell lysates according to the manufacturer's protocol (Zymo Research,
467 Tustin, CA). A High-Capacity cDNA Reverse Transcription Kit (Thermo Fisher Scientific, Waltham,
468 MA) was used for first-strand cDNA synthesis with 1 μg of total RNA from each sample. The expression

469 of genes and the GAPDH internal control was assayed by qPCR using SYBR Green (Bioline Reagents
470 Ltd, London, UK). Primer sequences are shown in **Table S1**.

471 **Immunoblotting**

472 Protein extracts were prepared using RIPA lysis buffer (Merck Millipore, Temecula, CA) containing
473 protease inhibitor cocktail and phosphatase inhibitor tablets (Sigma, MO, USA). Protein content was
474 determined using a protein assay kit (Bio-Rad, Hercules, CA). Western blotting was performed as
475 described previously (Wang et al., 2019). All primary (1:1000) and secondary antibodies (1:2000),
476 except BEST4 (1:800; LsBio, Seattle, WA) and anti-Flag M2 (Sigma, MO, USA), were purchased from
477 Cell Signaling Technology (Danvers, MA, USA).

478 **Cell proliferation**

479 Cell proliferation was monitored in real time using an *IncuCyte* ZOOM live-cell microscope
480 incubator (Essen Bioscience, MI, USA), in which the cell confluence was calculated using *IncuCyte*
481 software, and the cell proliferation was expressed as the percentage of confluence. According to the
482 manufacturer's protocol, a Cell Counting Kit-8 (CCK-8, Dojindo, Tokyo, Japan) assay was used to
483 confirm cell viability. The absorbance at 450 nm was measured using a microplate reader (BioTek, VT,
484 USA), and growth curves were drawn according to the optical density.

485 **Clonogenesis**

486 A total of 3×10^3 cells per well were seeded in 6-well plates. The medium was refreshed twice a
487 week. After 2 weeks, colonies were fixed and stained with crystal violet (0.005% in 20% methanol). The

488 numbers of colonies were quantified using GelCount (Oxford Optronix Ltd, Oxford, UK). The assay was
489 carried out in triplicate wells for three independent experiments.

490 **Transwell migration and invasion**

491 Cells were digested and suspended in culture medium without FBS for the migration assay. Cell
492 suspensions were added into the upper chamber of the Transwell insert and then placed into the 24-well
493 plate Transwell containing medium with 10% FBS in the lower chamber. For the invasion assay, the 24-
494 well plate with Transwell inserts was coated with 50 μg/insert of Matrigel matrix on the top of the
495 chamber (BD Biosciences, Oxford, UK). After 48 h, cells that travelled to the lower surface of the insert
496 were stained with crystal violet. Experiments were conducted in triplicate.

497 **Immunohistochemistry**

498 Paraffin-embedded tissue blocks from formalin-fixed tumour samples were sectioned, dewaxed,
499 and rehydrated following standard protocols. Sections were stained for human Ki67 primary antibody
500 (1:200, Cell Signaling Technology, MA, USA), a marker of cell proliferation, and anti-mouse HRP-
501 conjugated secondary antibody (Dako, CA, USA), and the positive cells were counted in eight randomly
502 chosen fields. Expression of BEST4-HA in tumours was stained with anti-HA primary antibody (1:800,
503 Cell Signaling Technology) and anti-rabbit HRP-conjugated secondary antibody (Dako).

504 **Dual-luciferase reporter assay**

505 The *BEST4* promoter region (−2000 to +100 bp) was cloned into pGL3-basic vectors (Promega, WI,
506 USA) to construct the luciferase reporter plasmid (pGL3-*BEST4*). The stably high Hes4 expression cell

507 line was constructed by infecting HCT116 cells with lentivirus, and then the recombinant plasmid pGL3-
508 *BEST4* was co-transfected with the control plasmid pRL-TK (Promega) into HCT116 Hes4 and HCT116
509 EV cells. Twenty-four hours after transfection, firefly and Renilla luciferase activities were analysed
510 using the dual-luciferase reporter assay (Promega) according to the manufacturer's instructions, and the
511 results were normalized as relative luciferase activity (firefly luciferase/Renilla luciferase).

512 **Chromatin immunoprecipitation-quantitative PCR (ChIP-qPCR)**

513 ChIP-qPCR was performed as previously described (Miotto and Struhl, 2006). At room temperature,
514 we crosslinked cells at 5×10^7 cells/mL for 10 min using 1% formaldehyde and stopped the reaction using
515 125 mM glycine. After three washes with ice-cold PBS, cells were homogenized, lysed, and sonicated
516 to shear DNA into 200–500 bp fragments. The DNA fragments were incubated with 10 μg of antibodies
517 against anti-Flag tag (Sigma, MO, USA) or native IgG (Cell Signaling Technology) followed by IP with
518 60 μl of protein A/G Magnetic Beads (MedChemExpress, New Jersey, USA) and overnight incubation
519 at 4 °C with rotation. Immunoprecipitated DNAs were extracted from the DNA/antibody/protein A/G
520 bead complexes using proteinase K digestion, subjected to reverse crosslinking at 65 °C for 4 h, and
521 purified with spin columns. qPCR analysis was performed to determine the enrichment of DNA
522 fragments using the indicated primers (**Table S1**). ChIP-qPCR data were normalized using the fold-
523 enrichment method (ChIP signals were divided by IgG signals), and DHFR 5 'UTR was used as a
524 negative control. Each experiment included triplicate samples and the data shown represent the mean of
525 three independent experiments.

526

527 **Immunofluorescence staining**

528 HCT116 cells transfected alone or co-transfected with expression vectors encoding C-terminal HA-
529 tagged BEST4, and N-terminal Flag-tagged Hes4 were grown on glass coverslips, fixed for 10 min with
530 4% paraformaldehyde, permeabilized for 5 min with 0.2% Triton X-100, then blocked for 15 min with
531 3% bovine serum albumin. HA-tagged *BEST4* was stained using an anti-HA antibody (Cell Signaling
532 Technology) followed by a TRITC-labelled secondary antibody (Abcam, Cambridge, UK). Flag-tagged
533 Hes4 was detected using an anti-Flag antibody (Sigma, MO, USA) with an Alexa Fluor 647-labeled
534 secondary antibody (Invitrogen Carlsbad, CA). Cells were mounted and imaged using laser-scanning
535 confocal microscopy (*Nikon* Corporation, Tokyo, Japan).

536 **Co-immunoprecipitation (Co-IP)**

537 Co-IP assays were performed on nuclear extracts. According to the manufacturer's protocols,
538 nuclear proteins of each sample were collected using Minute™ Cytoplasmic and Nuclear Fractionation
539 Kit (Invent, MN, USA). Protein G Dynabeads (Thermo Fisher Scientific, MA, USA) following the
540 manufacturer's instructions. Briefly, HEK293 cells were co-transfected with expression vectors encoding
541 C-terminal HA-tagged *BEST4* and N-terminal Flag-tagged Hes4. Cells were harvested and lysed 48 h
542 after transfection. Cell lysates (500 μg) were incubated overnight at 4 °C in a rotating wheel with 2 μg
543 of anti-FLAG (Sigma, MO, USA) or anti-HA antibody (Cell Signaling Technology) bound to Protein G
544 Dynabeads. Immunocomplexes were separated using a magnet, washed three times in PBS with 0.02%
545 Tween™ 20 and eluted in elution buffer (50 mM glycine pH 2.8). After boiling in sample buffer at
546 70 °C for 10 min, immunocomplexes were loaded on 4–20% Tris-glycine gels (Bio-Rad, CA, USA),
547 followed by blotting on PVDF membranes and immunoblotting using the indicated antibodies.

548 **Chloride channel efflux**

549 Cells were maintained in a serum free DMEM overnight prior to treatment with DIDS (4,4'-
550 diisothiocyanatostilbene-2,2'-disulfonic acid; HY-D0086, MCE, China), $CaCC_{inh}$-A01 (HY-100611,
551 MCE, China) or 1 μM ionomycin for 24h as previously published (Liu *et al*, 2015; Uwada *et al*, 2019).
552 Chloride channel efflux was evaluated with colorimetric changes by commercially available kits
553 (ab176767, Abcam). Briefly, 40,000 *BEST4*-expressing or *EV*-control HCT116 cells were plated per well
554 in a 96-well plate and allowed to grow over night. Before the assay, cells were refreshed with serum-free
555 medium and 100 μL/well of pre-warmed iodide-loading buffer was added and the plate was incubated
556 for 2 hours at 37 °C. After washing each well with HBSS three times, cells were lysed and Iodide Sensor
557 Blue dye (50 μL/well) and 0.5 x Iodide Sensor Enhancer (50 μL/well) were added and incubated for 1
558 minutes before reading at 405 nm. Data was calculated as fold-change relative to control.

559 **Statistical analysis**

560 The results were expressed as the mean ± standard error of the mean. The statistical significance of
561 differences between means was assessed using Student's unpaired two-tailed *t*-tests, and the Mann-
562 Whitney U test was performed to compare the variables in two groups using SPSS 25.0 (SPSS, Chicago,
563 USA). The relationship between the clinicopathological parameters of CRC and the expression of *BEST4*
564 was examined using the Kruskal-Wallis H test. The Kaplan-Meier method and log-rank tests were used
565 to assess overall survival in relation to *BEST4* expression. Differences in cell proliferation and tumour
566 growth rates between the two groups of mice were assessed using repeated-measures analysis of variance.

Western blot intensity was assessed using ImageJ v1.53 software (ImageJ, Bethesda, MD, USA). *P*-values <0.05 indicated statistically significant differences.

Data and code availability: The raw sequence data reported in this paper have been deposited in the NCBI Sequence Read Archive (SRA) with accession number PRJNA690126.

Compliance and ethics: The author(s) declare that they have no conflict of interest. The clinical studies were approved by the Ethics Committee of West China Hospital, Sichuan University (Sichuan, China). All procedures were performed per the 1964 Declaration of Helsinki. Written informed consent was obtained from all participants. The Animal Ethics Committee approved animal experiments of West China Hospital, Sichuan University (Sichuan, China).

Acknowledgments: We thank Xuemei Cheng, Sisi Wu, and Huifang Li from Core Facilities of West China Hospital, Sichuan University, for expert technical assistance. This work was supported by the National Natural Science Foundation of China (grant numbers: 82173253, 82103539, 82074298), Sichuan Science and Technology Program (grant numbers: 2021YFH0005, 2022YFH0003), Sichuan Province cadres health research project (grant numbers: 2023104).

586 **References**

587 Acloque, H., Adams, M.S., Fishwick, K., Bronner-Fraser, M., and Nieto, M.A. (2009). "Epithelial-
588 mesenchymal transitions: the importance of changing cell state in development and disease". J Clin
589 Invest *119*, 1438-1449. 10.1172/JCI38019.
590 Bulzico, D., Pires, B.R.B., PAS, D.E.F., Neto, L.V., and Abdelhay, E. (2019). "Twist1 Correlates With
591 Epithelial-Mesenchymal Transition Markers Fibronectin and Vimentin in Adrenocortical Tumors".
592 Anticancer research *39*, 173-175. 10.21873/anticanres.13094.
593 Cakouros, D., Isenmann, S., Hemming, S.E., Menicanin, D., Camp, E., Zannetinno, A.C., and
594 Gronthos, S. (2015). "Novel basic helix-loop-helix transcription factor hes4 antagonizes the function of
595 twist-1 to regulate lineage commitment of bone marrow stromal/stem cells". Stem Cells Dev *24*, 1297-
596 1308. 10.1089/scd.2014.0471.
597 Dongre, A., and Weinberg, R.A. (2019). "New insights into the mechanisms of epithelial-mesenchymal
598 transition and implications for cancer". Nature reviews. Molecular cell biology *20*, 69-84.
599 10.1038/s41580-018-0080-4.
600 El Yakoubi, W., Borday, C., Hamdache, J., Parain, K., Tran, H.T., Vleminckx, K., Perron, M., and
601 Locker, M. (2012). "Hes4 controls proliferative properties of neural stem cells during retinal
602 ontogenesis". Stem cells (Dayton, Ohio) *30*, 2784-2795. 10.1002/stem.1231.
603 Fagerberg, L., Hallström, B.M., Oksvold, P., Kampf, C., Djureinovic, D., Odeberg, J., Habuka, M.,
604 Tahmasebpoor, S., Danielsson, A., Edlund, K., et al. (2014). "Analysis of the human tissue-specific
605 expression by genome-wide integration of transcriptomics and antibody-based proteomics". Mol Cell
606 Proteomics *13*, 397-406. 10.1074/mcp.M113.035600.
607 Huang, F., Wong, X., and Jan, L.Y. (2012). "International Union of Basic and Clinical Pharmacology.
608 LXXXV: calcium-activated chloride channels". Pharmacological reviews *64*, 1-15.
609 10.1124/pr.111.005009.
610 Ito, G., Okamoto, R., Murano, T., Shimizu, H., Fujii, S., Nakata, T., Mizutani, T., Yui, S., Akiyama-
611 Morio, J., Nemoto, Y., et al. (2013). "Lineage-specific expression of bestrophin-2 and bestrophin-4 in
612 human intestinal epithelial cells". PLoS One *8*, e79693. 10.1371/journal.pone.0079693.

613 Katoh, M., and Katoh, M. (2004). "Identification and characterization of human HES2, HES3, and
614 HES5 genes in silico". International journal of oncology *25*, 529-534.
615 Li, X., Hu, W., Zhou, J., Huang, Y., Peng, J., Yuan, Y., Yu, J., and Zheng, S. (2017). "CLCA1
616 suppresses colorectal cancer aggressiveness via inhibition of the Wnt/beta-catenin signaling pathway".
617 Cell communication and signaling : CCS *15*, 38. 10.1186/s12964-017-0192-z.
618 Liu, Y., Zhang, H., Huang, D., Qi, J., Xu, J., Gao, H., Du, X., Gamper, N., and Zhang, H. (2015).
619 "Characterization of the effects of Cl^- channel modulators on TMEM16A and bestrophin-1 Ca^{2+}
620 activated Cl^- channels". Pflugers Archiv : European journal of physiology *467*, 1417-1430.
621 10.1007/s00424-014-1572-5.
622 M. B. Amin et al. (Springer, 2017). "AJCC Cancer Staging Manual".
623 Marmorstein, A.D., Cross, H.E., and Peachey, N.S. (2009). "Functional roles of bestrophins in ocular
624 epithelia". Progress in retinal and eye research *28*, 206-226. 10.1016/j.preteyeres.2009.04.004.
625 Matchkov, V.V., Larsen, P., Bouzinova, E.V., Rojek, A., Boedtkjer, D.M., Golubinskaya, V., Pedersen,
626 F.S., Aalkjaer, C., and Nilsson, H. (2008). "Bestrophin-3 (vitelliform macular dystrophy 2-like 3
627 protein) is essential for the cGMP-dependent calcium-activated chloride conductance in vascular
628 smooth muscle cells". Circ Res *103*, 864-872. 10.1161/circresaha.108.178517.
629 Meng, J., Chen, S., Han, J.X., Qian, B., Wang, X.R., Zhong, W.L., Qin, Y., Zhang, H., Gao, W.F., Lei,
630 Y.Y., et al. (2018). "Twist1 Regulates Vimentin through Cul2 Circular RNA to Promote EMT in
631 Hepatocellular Carcinoma". Cancer research *78*, 4150-4162. 10.1158/0008-5472.Can-17-3009.
632 Milenkovic, V.M., Langmann, T., Schreiber, R., Kunzelmann, K., and Weber, B.H. (2008). "Molecular
633 evolution and functional divergence of the bestrophin protein family". BMC evolutionary biology *8*,
634 72. 10.1186/1471-2148-8-72.
635 Miller, A.N., Vaisey, G., and Long, S.B. (2019). "Molecular mechanisms of gating in the calcium-
636 activated chloride channel bestrophin". eLife *8*. 10.7554/eLife.43231.
637 Miotto, B., and Struhl, K. (2006). "Differential gene regulation by selective association of
638 transcriptional coactivators and bZIP DNA-binding domains". Molecular and cellular biology *26*,
639 5969-5982. 10.1128/MCB.00696-06.

Murato, Y., and Hashimoto, C. (2009). "Xhairy2 functions in Xenopus lens development by regulating p27(xic1) expression". Developmental dynamics : an official publication of the American Association of Anatomists *238*, 2179-2192. 10.1002/dvdy.21883.

Nagai, T., Arao, T., Nishio, K., Matsumoto, K., Hagiwara, S., Sakurai, T., Minami, Y., Ida, H., Ueshima, K., Nishida, N., et al. (2016). "Impact of Tight Junction Protein ZO-1 and TWIST Expression on Postoperative Survival of Patients with Hepatocellular Carcinoma". Digestive diseases (Basel, Switzerland) *34*, 702-707. 10.1159/000448860.

Nichane, M., de Crozé, N., Ren, X., Souopgui, J., Monsoro-Burq, A.H., and Bellefroid, E.J. (2008). "Hairy2-Id3 interactions play an essential role in Xenopus neural crest progenitor specification". Developmental biology *322*, 355-367. 10.1016/j.ydbio.2008.08.003.

Parikh, K., Antanaviciute, A., Fawkner-Corbett, D., Jagielowicz, M., Aulicino, A., Lagerholm, C., Davis, S., Kinchen, J., Chen, H.H., Alham, N.K., et al. (2019). "Colonic epithelial cell diversity in health and inflammatory bowel disease". Nature *567*, 49-55. 10.1038/s41586-019-0992-y.

Pastushenko, I., and Blanpain, C. (2019). "EMT Transition States during Tumor Progression and Metastasis". Trends in cell biology *29*, 212-226. 10.1016/j.tcb.2018.12.001.

Pifferi, S., Dibattista, M., Sagheddu, C., Boccaccio, A., Al Qteishat, A., Ghirardi, F., Tirindelli, R., and Menini, A. (2009). "Calcium-activated chloride currents in olfactory sensory neurons from mice lacking bestrophin-2". The Journal of physiology *587*, 4265-4279. 10.1113/jphysiol.2009.176131.

Porretti, J., Dalton, G.N., Massillo, C., Scalise, G.D., Farré, P.L., Elble, R., Gerez, E.N., Accialini, P., Cabanillas, A.M., Gardner, K., et al. (2018). "CLCA2 epigenetic regulation by CTBP1, HDACs, ZEB1, EP300 and miR-196b-5p impacts prostate cancer cell adhesion and EMT in metabolic syndrome disease". International journal of cancer *143*, 897-906. 10.1002/ijc.31379.

Qu, H., Su, Y., Yu, L., Zhao, H., and Xin, C. (2019). "Wild-type p53 regulates OTOP2 transcription through DNA loop alteration of the promoter in colorectal cancer". FEBS open bio *9*, 26-34. 10.1002/2211-5463.12554.

Rawla, P., Sunkara, T., and Barsouk, A. (2019). "Epidemiology of colorectal cancer: incidence, mortality, survival, and risk factors". Przeglad gastroenterologiczny *14*, 89-103. 10.5114/pg.2018.81072.

Roger, L., Jullien, L., Gire, V., and Roux, P. (2010). "Gain of oncogenic function of p53 mutants regulates E-cadherin expression uncoupled from cell invasion in colon cancer cells". Journal of cell science *123*, 1295-1305. 10.1242/jcs.061002.

Sanders, K.M., Zhu, M.H., Britton, F., Koh, S.D., and Ward, S.M. (2012). "Anoctamins and gastrointestinal smooth muscle excitability". Exp Physiol *97*, 200-206. 10.1113/expphysiol.2011.058248.

Sui, Y., Sun, M., Wu, F., Yang, L., Di, W., Zhang, G., Zhong, L., Ma, Z., Zheng, J., Fang, X., and Ma, T. (2014). "Inhibition of TMEM16A expression suppresses growth and invasion in human colorectal cancer cells". PLoS One *9*, e115443. 10.1371/journal.pone.0115443.

Sun, L., Ke, J., He, Z., Chen, Z., Huang, Q., Ai, W., Wang, G., Wei, Y., Zou, X., Zhang, S., et al. (2017). "HES1 Promotes Colorectal Cancer Cell Resistance To 5-Fu by Inducing Of EMT and ABC Transporter Proteins". Journal of Cancer *8*, 2802-2808. 10.7150/jca.19142.

Sunlin Yong, Z.W., Tang Yuan, Chuang Cheng, Dan Jiang (2021). "Comparison of MMR protein and Microsatellite Instability Detection in Colorectal Cancer and Its Clinicopathological Features Analysis". Journal of Medical Research *50*, 61-66. 10.11969/j.issn.1673-548X.2021.05.015

Tsunenari, T., Sun, H., Williams, J., Cahill, H., Smallwood, P., Yau, K.W., and Nathans, J. (2003). "Structure-function analysis of the bestrophin family of anion channels". The Journal of biological chemistry *278*, 41114-41125. 10.1074/jbc.M306150200.

Uwada, J., Yazawa, T., Nakazawa, H., Mikami, D., Krug, S.M., Fromm, M., Sada, K., Muramatsu, I., and Taniguchi, T. (2019). "Store-operated calcium entry (SOCE) contributes to phosphorylation of p38 MAPK and suppression of TNF-α signalling in the intestinal epithelial cells". Cellular signalling *63*, 109358. 10.1016/j.cellsig.2019.109358.

van Es, J.H., van Gijn, M.E., Riccio, O., van den Born, M., Vooijs, M., Begthel, H., Cozijnsen, M., Robine, S., Winton, D.J., Radtke, F., and Clevers, H. (2005). "Notch/gamma-secretase inhibition turns proliferative cells in intestinal crypts and adenomas into goblet cells". Nature *435*, 959-963. 10.1038/nature03659.

694 Vesuna, F., van Diest, P., Chen, J.H., and Raman, V. (2008). "Twist is a transcriptional repressor of E-
695 cadherin gene expression in breast cancer". Biochem Biophys Res Commun *367*, 235-241.
696 10.1016/j.bbrc.2007.11.151.
697 Walia, V., Yu, Y., Cao, D., Sun, M., McLean, J.R., Hollier, B.G., Cheng, J., Mani, S.A., Rao, K.,
698 Premkumar, L., and Elble, R.C. (2012). "Loss of breast epithelial marker hCLCA2 promotes epithelial-
699 to-mesenchymal transition and indicates higher risk of metastasis". Oncogene *31*, 2237-2246.
700 10.1038/onc.2011.392.
701 Wang, Z., Kawaguchi, K., Honda, M., Hashimoto, S., Shirasaki, T., Okada, H., Orita, N., Shimakami,
702 T., Yamashita, T., Sakai, Y., et al. (2019). "Notch signaling facilitates hepatitis B virus covalently
703 closed circular DNA transcription via cAMP response element-binding protein with E3 ubiquitin
704 ligase-modulation". Scientific reports *9*, 1621. 10.1038/s41598-018-38139-5.
705 Yang, B., Cao, L., Liu, J., Xu, Y., Milne, G., Chan, W., Heys, S.D., McCaig, C.D., and Pu, J. (2015).
706 "Low expression of chloride channel accessory 1 predicts a poor prognosis in colorectal cancer".
707 Cancer *121*, 1570-1580. 10.1002/cncr.29235.
708 Yang, J., Mani, S.A., Donaher, J.L., Ramaswamy, S., Itzykson, R.A., Come, C., Savagner, P.,
709 Gitelman, I., Richardson, A., and Weinberg, R.A. (2004). "Twist, a master regulator of morphogenesis,
710 plays an essential role in tumor metastasis". Cell *117*, 927-939. 10.1016/j.cell.2004.06.006.
711 Yeung, K.T., and Yang, J. (2017). "Epithelial-mesenchymal transition in tumor metastasis". Molecular
712 oncology *11*, 28-39. 10.1002/1878-0261.12017.
713 Yu, X., Li, S., Xu, Y., Zhang, Y., Ma, W., Liang, C., Lu, H., Ji, Y., Liu, C., Chen, D., and Li, J. (2020).
714 "Androgen Maintains Intestinal Homeostasis by Inhibiting BMP Signaling via Intestinal Stromal
715 Cells". Stem cell reports *15*, 912-925. 10.1016/j.stemcr.2020.08.001.
716 Yuan, R., Ke, J., Sun, L., He, Z., Zou, Y., He, X., Chen, Y., Wu, X., Cai, Z., Wang, L., et al. (2015).
717 "HES1 promotes metastasis and predicts poor survival in patients with colorectal cancer". Clinical &
718 experimental metastasis *32*, 169-179. 10.1007/s10585-015-9700-y.
719 Yusup, A., Huji, B., Fang, C., Wang, F., Dadihan, T., Wang, H.J., and Upur, H. (2017). "Expression of
720 trefoil factors and TWIST1 in colorectal cancer and their correlation with metastatic potential and
721 prognosis". World journal of gastroenterology *23*, 110-120. 10.3748/wjg.v23.i1.110.

Zhang, L., Cao, F., Zhang, G., Shi, L., Chen, S., Zhang, Z., Zhi, W., and Ma, T. (2019). "Trends in and Predictions of Colorectal Cancer Incidence and Mortality in China From 1990 to 2025". Frontiers in oncology *9*, 98. 10.3389/fonc.2019.00098.

Zhang, N., Ng, A.S., Cai, S., Li, Q., Yang, L., and Kerr, D. (2021). "Novel therapeutic strategies: targeting epithelial-mesenchymal transition in colorectal cancer". The Lancet. Oncology *22*, e358-e368. 10.1016/s1470-2045(21)00343-0.

Zhu, D.J., Chen, X.W., Zhang, W.J., Wang, J.Z., Ouyang, M.Z., Zhong, Q., and Liu, C.C. (2015). "Twist1 is a potential prognostic marker for colorectal cancer and associated with chemoresistance". American journal of cancer research *5*, 2000-2011.

743 **Figure legends**

744 **Figure 1.** *BEST4* inhibits CRC cell proliferation, clonogenesis, migration, and invasion in vitro.
745 Overexpression of *BEST4* decreased proliferation of HCT 116 (A) and Caco2 (B) cells as determined by
746 the IncuCyte confluence assay. (C) Viability of three individual *BEST4*-deleted clones as determined by
747 a CCK-8 assay. (D) *BEST4* deletion significantly enhanced cell viability compared with cells transduced
748 with EV-gRNA control; the reintroduction of *BEST4* resulted in suppressed cell growth as determined
749 by IncuCyte confluence analysis. (E) Expression of *BEST4*-HA in HCT116 and Caco2 cells resulted in
750 more colonies than cells transduced with EV plasmids (left panel); colonies were counted and analysed
751 as shown (right panel). (F) A colony formation assay was performed to evaluate the responses of HCT-
752 15 cells following *BEST4* deletion and reintroduction (left panel); cell colonies were counted and
753 analysed as shown (right panel). (G) Heterologous expression of BEST4 in HCT116 cells suppressed
754 invasion and migration (upper panel, scale bar, 200 μm); cells that passed through the membrane were
755 counted and compared (lower panel). (H) *BEST4* deletion in HCT-15 cells promoted invasion, whereas
756 reintroduction of *BEST4* expression resulted in the inhibition of HCT-15 cell invasion and migration
757 (upper panel, scale bar, 200 μm). Cells that passed through the membrane were counted and compared
758 (lower panel). Data shown are the result of at least three independent experiments, with the mean ± SEM;
759 *$P<0.05$, **$P<0.01$ vs EV or WT.

760 **Figure 2.** *BEST4* deters EMT in CRC in vitro and *in vivo.* (A) Expression of mRNAs encoding EMT-
761 related genes as determined by qPCR in HCT116 cells transfected with BEST4-HA or EV. (B) As
762 determined by qPCR, the expression of mRNAs encoding EMT markers in *BEST4*-deleted and *BEST4*-

763 restored HCT-15 cells. (C) Protein expression of EMT-related genes was evaluated by western blotting
764 of lysates of HCT116 cells transfected with BEST4-HA or EV. (D) Western blotting determined the
765 levels of immunoreactive EMT markers in *BEST4*-deleted and *BEST4*-restored HCT-15 cells. (E)
766 Growth of xenograft tumours in BALB/c nude mice resulting from the injection of HCT116 cells stably-
767 transduced with *BEST4*-HA was significantly diminished compared with those resulting from HCT116
768 cells transduced with EV alone (eight mice per group). (F) The histogram represents the mean weights
769 of tumours isolated from the HCT116-*BEST4*-HA and HCT116-EV groups. (G) Tumours from the
770 HCT116-*BEST4*-HA and HCT116-EV groups were sectioned and subjected to immunohistochemical
771 staining to detect HA and human Ki67; scale bar=50 μm. (H) Mean percentage of Ki67-positive staining
772 in each group. (I) Representative western blot documenting protein levels of EMT markers in individual
773 HCT116-BEST4 and HCT116-EV xenograft tumours. (J) Each band's mean pixel intensities were
774 determined and normalized to mean β-actin pixel intensity. *P<0.05, **P<0.01. Data from at least three
775 independent experiments are presented as the mean ± SEM. (K and J) Intrasplenical injections of HCT-
776 15 cell lines with EV-gRNA control, BEST4-gRNA or BEST4-Rescued (n = 3 per group). After 28 days,
777 the animals were sacrificed and numbers of metastatic nodules in the liver were counted, and the liver
778 tissues were fixed for sectioning and H&E staining. Data are presented as the mean ± SEM. **P<0.01
779 vs EV-gRNA.

780 **Figure 3.** Molecular regulation of BEST4 expression by Hes4. (A) Endogenous *BEST4* mRNA and
781 protein levels in *Hes4*-overexpressing HCT116 cells were detected by qPCR and western blotting,
782 respectively. (B) Endogenous *BEST4* mRNA and protein levels in LS174T cells after shRNA-mediated
783 Hes4 knockdown as detected by qPCR and western blotting, respectively. (C) Detection of *BEST4*

784 promoter activity in Hes4-overexpressing HCT116 cells using a dual-luciferase reporter assay. (D) As
785 determined by ChIP-qPCR, Fold-enrichment of the *BEST4* promoter region in Flag-ChIP samples from
786 Hes4-overexpressing HCT116 cells. Data were normalized using a fold-enrichment method (i.e., ChIP
787 signals divided by control IgG signals). The DHFR 5' UTR was used as a negative control (upper panel).
788 The primer sets that target the BEST4 promoter in the ChIP-qPCR assays are as illustrated; +1 marks the
789 transcriptional start site of *BEST4*, and P1, P2, P3, and P4 represent primer locations (lower panels). (E)
790 Immunofluorescence staining documents the colocalization of BEST4 (green) and Hes4 (red) in HCT116
791 cells based on detection of their specific tags; scale bar, 20 μM. (F) Co-immunoprecipitation of nuclear
792 extracts with specifically-tagged BEST4 and Hes4 as determined by immunoblotting. Lamin B1 served
793 as a nuclear protein control. (G) Detection of *BEST4* promoter activity in *Hes4*-overexpressing HCT116
794 cells after *BEST4* knockdown through a dual-luciferase reporter assay. Data shown are the result of at
795 least three independent experiments, with the mean ± SEM; *P<0.05, **P<0.01 vs EV

796 **Figure 4.** *BEST4* relays the Hes4 signal and directly downregulates Twist1 expression to counteract EMT
797 induction in CRC (A) Detection of Twist1 promoter activity in *Hes4*-overexpressing or *BEST4*-
798 overexpressing HCT116 cells through a dual-luciferase reporter assay. (B) Detection of Twist1 promoter
799 activity in *Hes4*-overexpressing HCT116 cells after BEST4 knockdown through a dual-luciferase
800 reporter assay. (C) Detection of Twist1 promoter activity in HCT116 cells after shRNA-mediated Hes4
801 knockdown and combination with *BEST4*-overexpressing using a dual-luciferase reporter assay. (D) Co-
802 immunoprecipitation of nuclear extracts with specifically-tagged BEST4 and Twist1 as determined by
803 immunoblotting. Lamin B1 served as a nuclear protein control. (E) Co-immunoprecipitation of nuclear
804 extracts with specifically-tagged Hes4 and Twist1 as determined by immunoblotting. Lamin B1 served

805 as a nuclear protein control. (F) Expression of EMT markers in *Hes4*-overexpressing HCT116 cells. (G)
806 Expression of EMT markers in LS174T cells after shRNA-mediated *Hes4* knockdown. (H) Expression
807 of EMT markers in *Hes4*-overexpressing HCT116 cells after BEST4 knockdown. (I) Expression levels
808 of EMT markers in *BEST4*-overexpressing LS174T cells after Hes4-knockdown; SCR, scrambled siRNA.

809 **Figure 5.** Correlation of the *BEST4* gene with clinicopathology and outcomes of patients diagnosed with
810 CRC. (A) Heatmap based on the top 100 differentially expressed genes (downregulated and upregulated)
811 in CRCs compared with ANTs. (B) Volcano plots of RNA seq results showing all differentially expressed
812 genes in CRC tissues compared with ANTs based on the fold-change ($|FC| \geq 1$) and *P-value (P*≤ 0.05). (C)
813 Expression levels of *BEST4* mRNA in 50 pairs of adenoma tissues compared with ANTs. (D) Expression
814 levels of *BEST4* mRNA in 124 pairs of CRC tissues compared with ANTs. (E) BEST4 protein levels in
815 CRC and their matched counterparts were measured using western blotting. (F) Kaplan-Meier survival
816 analysis according to *BEST4* expression in 124 patients with CRC. The difference was statistically
817 significant based on the log-rank test ($P<0.01$). (G) A working model delineates the mechanism by which
818 *BEST4* is transcriptionally activated by *Hes4* and suppressed EMT through Twist1 inhibition: a. the
819 expression of *BEST4* is regulated by interactions of its upstream promoter region with Hes4. *BEST4*
820 positively promotes the transcriptional activity of Hes4 on *BEST4* by physically binding to Hes4 in a
821 positive feedback loop; b. The complex formed by BEST4 and Hes4 interacts with Twist1 and inhibits
822 the promoter activity of Twist1. Hes4 alone is insufficient to inhibit Twist1 promoter activity, and BEST4
823 is required. Inhibition of Twist1 promoter activity by Hes4 is BEST4-dependent c. The complex formed
824 by BEST4 and Hes4 destabilized Twist1; the same effect caused by Hes4 required BEST4 intermediation.

825 The Hes4-BEST4-Twist1 axis counteracts EMT induction. *P<0.05, **P<0.01; CRC, colorectal cancer;

826 ANT, adjacent normal tissue; T, tumour.

827

828

829

830

831

832

833

834

835

836

837

838

839

840

841 **FIGURE SUPPLEMENT LEGENDS**

842 **Figure 1-supplemental figure 1.** Construction of *BEST4*-overexpressing /*BEST4*-depetion CRC cell
843 lines, and cell proliferation measured by CCK-8 assay. (A) HA protein expression in *BEST4*-HA-
844 transfected GFP^+ HCT116 individual clonal lines. (B) HA protein expression in *BEST4*-HA-transfected
845 GFP^+ Caco2 individual clonal lines. (C) *BEST4* mRNA and HA protein expression was detected by real-
846 time PCR and western blotting. (D) Cell viability in *BEST4*-HA- and EV-transfected HCT116 cells was
847 measured by the CCK-8 assay. (E) Cell viability in *BEST4*-HA- and EV-transfected Caco2 cells was
848 measured by the CCK-8 assay. (F) DNA sequencing results revealed an excision of a 44-bp genomic
849 fragment in exon 3 of the *BEST4*-knockout lines. (G) DNA fragmentation from each sample was analysed
850 by agarose gel electrophoresis. (H) The protein level of BEST4 was determined by western blotting. (H)
851 Cell proliferation measured by CCK-8 assay showed that knockout of *BEST4* obviously promoted cell
852 growth; however, rescue of *BEST4* expression in the knockout cells significantly abrogated the promotive
853 effect of *BEST4* knockout on cell growth. $^{*}P<0.05$, $^{**}P<0.01$. All the data come from three independent
854 experiments and are presented as the mean ± standard deviation.

855 **Figure 3-supplemental figure 1.** *BEST4* interacted with *Hes4*. (A) *Hes4* mRNA and protein levels in
856 HCT116 cells with *Hes4* overexpression by Flag-*Hes4* transfection and (B) LS174T cells with *Hes4*
857 knockdown by shRNA transfection were examined by real-time PCR and western blot. (C) No significant
858 change of *Hes4* mRNA levels in *BEST4*-overexpression HCT116 cells as detected by real-time PCR. (D)
859 *BEST4* mRNA levels in HCT116 and LS174T cells transfected with *BEST4*-specific siRNAs as detected
860 by real-time PCR. $^{*}P<0.05$, $^{**}P<0.01$. All the data come from three independent experiments and are
861 presented as the mean ± SEM. SRC, scramble siRNA.

862 **Figure 4-supplemental figure 1.** *BEST4* interacted with *Hes4* to inhibit Twist1. (A) Co-
863 immunoprecipitation of nuclear extracts with specifically-tagged BEST4 and Twist1 as determined by
864 immunoblotting, Lamin B1 served as a nuclear protein control. (B) Co-immunoprecipitation of nuclear
865 extracts with specifically-tagged Hes4 and Twist1 as determined by immunoblotting, Lamin B1 served
866 as a nuclear protein control. (C) *Vimentin* mRNA levels in *Hes4*-overexpression HCT 116 cell lines as
867 detected by real-time PCR. (D) *Vimentin* mRNA levels in *Hes4*-overexpression HCT 116 cell lines after
868 *BEST4* knockdown as detected by real-time PCR. $^{*}P<0.05$, $^{**}P<0.01$. All the data were generated from
869 three independent experiments and are presented as the mean ± SEM. SRC, scramble siRNA.

870 **Figure 5-supplemental figure 4.** *BEST4* suppresses EMT independently of its channel functions. (A-C)
871 Incubation of HCT116 cell lines expressed BEST4 or EV with DIDS (300μM), a gradient increased
872 CaCCinh-A01 and ionomycin (1μM), respectively, overnight. The levels of chloride efflux were
873 determined by calculating relative fold to the EV control. Data are shown as means ± SEM, $p < 0.05$ vs
874 EV or DIDS, or CaCCinh-A01 or ionomycin, with 3 independent experiments. (D-F) Following the same
875 treatment, cell lysates were prepared for immunoblotting with antibodies to BEST4, ZO-1, E-cadherin,
876 Twist1 and β-actin. Representative 3 independent experiments.

877 **Figure 6-supplemental figure 1.** *BEST4* mRNA expression in colorectal tumours and matched non-
878 tumour tissues and the clinical relationship between *BEST4*, *Hes4* and EMT markers. (A) Correlation
879 between *BEST4* and *CDH1* in normal and colorectal cancer samples analysed from the TCGA and GTEx
880 databases using the GEPIA tool (http://gepia.cancer-pku.cn/). (B) RNA-seq data revealed decreased
881 expression of and *Hes4* in CRC tissues compared with ANTs. (C) Heatmap of *Hes4* expression in CRC

882 and ANTs. (D) The correlation between *BEST4* and *Hes4*, in CRC analysed from the TCGA and GTEx
883 databases using GEPIA (http://gepia.cancer-pku.cn/). (E) Correlation between *BEST4* and *CDH1* in
884 normal and colorectal cancer samples analysed from the TCGA and GTEx databases using the GEPIA
885 tool (http://gepia.cancer-pku.cn/). (F) Correlation between *BEST4* and *vimentin* in normal and colorectal
886 cancer samples. (G) Correlation between *BEST4* and Twist1 in normal and cancer colorectal samples.
887 ANT, adjacent normal tissues; COAD, colon adenocarcinoma; READ, rectum adenocarcinoma; other
888 tumour abbreviations are available at GEPIA: http://gepia.cancer-pku.cn/.

889 **Key resources table**

REAGENT or RESOURCE	SOURCE	IDENTIFIER
Antibodies		
BEST4	LsBio	Cat# LS-C31133-100, RRID:AB_911624
Hes4	Santa Cruz	Cat# sc-376002, RRID:AB_10987629
Flag	Sigma-Aldrich	Cat# F3165, RRID:AB_259529)
HA	Cell Signaling Technology	Cat# 3724, RRID:AB_1549585
ZO-1	Cell Signaling Technology	Cat# 8193, RRID:AB_10898025
E-Cadherin	Cell Signaling Technology	Cat# 3195, RRID:AB_2291471
Vimentin	Cell Signaling Technology	Cat# 5741, RRID:AB_1069545

Twist1	Cell Signaling Technology	Cat# 46702, RRID:AB_279930
Mouse (G3A1) mAb IgG1	Cell Signaling Technology	Cat# 5415, RRID:AB_10829607
Normal rabbit IgG	Cell Signaling Technology	Cat# 2729, RRID:AB_103106
Ki-67	Cell Signaling Technology	Cat# 9449, RRID:AB_2797703
Alexa Fluor 647	Invitrogen	Cat# A-21235, RRID:AB_2535804
TRITC	Abcam	Cat# ab6718, RRID:AB_955551
Anti-rabbit IgG	Cell Signaling Technology	Cat# 14708, RRID:AB_2798581
Anti-mouse IgG	Cell Signaling Technology	Cat# 14709, RRID:AB_2798582
HRP-conjugated secondary antibody	Dako	Cat# P0447, RRID:AB_2617137
β-actin	Cell Signaling Technology	Cat# 3700, RRID:AB_2242334
Lamin B1	Cell Signaling Technology	Cat# 17467, RRID:AB_ 10896336
Biological samples		
Human colorectal cancer samples	West China Hospital of Sichuan University	N/A
Chemicals, peptides, and recombinant proteins		
Direct-zol RNA Kit	Zymo Research	Cat# R2050

High-Capacity cDNA Reverse Transcription Kit	Thermo Fisher Scientific	Cat# 4368814
SYBR Green	Bioline Reagents Ltd,	Cat# RR036A
RIPA lysis buffer	Merck Millipore	Cat# P0013B
protease inhibitor cocktail	Sigma-Aldrich	Cat# P8340
phosphatase inhibitor	Sigma-Aldrich	Cat# P5726
Matrigel	BD Biosciences	Cat# 356234
Protein G Dynabeads	Thermo Fisher Scientific	Cat# 1009D
Protein A/G Magnetic Beads	MedChemExpress,	Cat# HY-K0202
DMEM	GIBCO Thermo Fisher Scientific	Cat# 31966
FBS	GIBCO Thermo Fisher Scientific	Cat# 10270
Lipofectamine 3000	Invitrogen	Cat# L3000001
puromycin	Invivogen	Cat# anti-pr
Critical commercial assays		
Cell Counting Kit-8 (CCK-8) assay	Dojindo	Cat# CK04
Protein assay kit	Bio-Rad,	Cat# 5000001
Dual-Luciferase Reporter Assay System	Promega	Cat #E1910
MycoAlert™ Mycoplasma Detection Kit	Lonza	Cat# LT07-318
Minute™ Cytoplasmic and Nuclear Fractionation Kit	Invent	Cat# SC-003
Deposited data		
RNA-seq data	NCBI SRA	RJNA690126

Experimental models: Cell lines and animals		
HCT116	ATCC	Cat# CCL-247
Caco2	ATCC	Cat# HTB-37
HCT-15	ATCC	Cat# CCL-225,
LS174T	ATCC	Cat# CCL-188
HEK293T	ATCC	Cat# CRL3216
BALB/c nude mice	Beijing HFK Bioscien ce	N/A
Oligonucleotides		
qPCR Primer sequences	See Table S1	N/A
shRNA sequences	See Table S1	N/A
siRNA sequences	See Table S1	N/A
ChIP-qPCR Primer sequences	See Table S1	N/A
Recombinant DNA		
Plasmid: pCDH-CMV-MCS-EF1-CopGFP-T2A-Puro	Public Protein/Plasmid Library	Cat# 030001
Plasmid: BEST4-HA-GFP	Public Protein/Plasmid Library	Cat# PPL01999-4b
Plasmid: pU6-gRNA-Cas9-EGFP	GenePharma	Cat# B5620
Plasmid: BEST4-gRNA	GenePharma	Cat# B5620
Plasmid: Flag-Hes4-GFP	Public Protein/Plasmid Library	Cat# PPL01973-4a
Plasmid: pGL3-basic vectors	Promega	Cat# E1751
Plasmid: pRL-TK	Promega	Cat# E2241

Plasmid: pGL3-BEST4	Public Protein/Plasmid Library	Cat# PPL01999-2a
Plasmid: pcDNA3.1	Public Protein/Plasmid Library	Cat# PE004
Plasmid: HES4-shRNA	Public Protein/Plasmid Library	Cat# PPL01973-3
Software and algorithms		
IncuCyte software	This paper	https://www.essenbioscience.com/
ImageJ	This paper	https://imagej.nih.gov/ij/
SPSS 25.0	This paper	www.ibm.com/software/analytics/spss

890

891

892

893

894

895

896

897

898

899

900 **Figure 1**

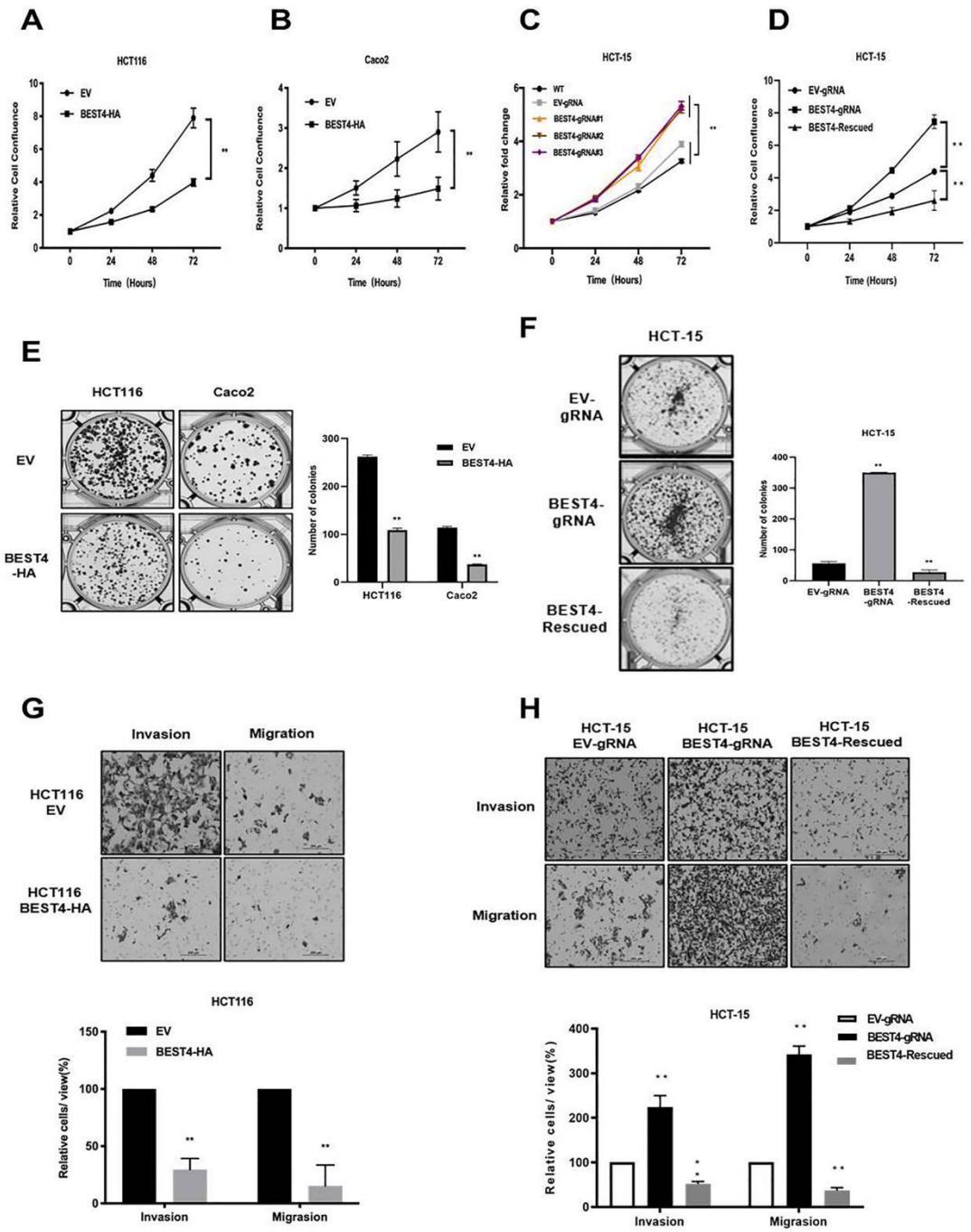

901

902

903

904

Figure 2

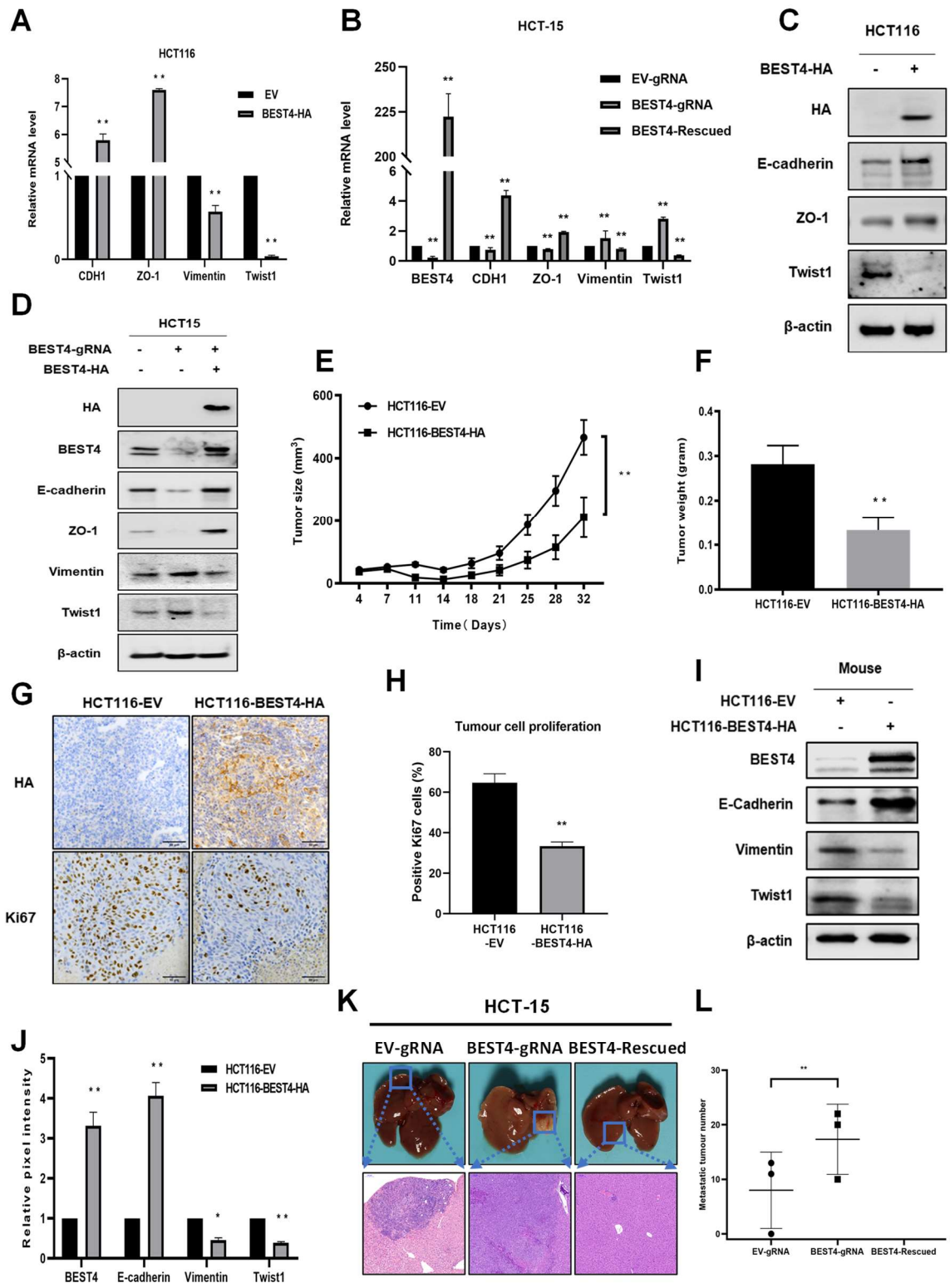
A
HCT116
Relative mRNA level
EV
BEST4-HA
CDH1
ZO-1
Vimentin
Twist1
B
HCT-15
Relative mRNA level
EV-gRNA
BEST4-gRNA
BEST4-Rescued
BEST4
CDH1
ZO-1
Vimentin
Twist1
C
HCT116
BEST4-HA
HA
E-cadherin
ZO-1
Twist1
β-actin
D
HCT15
BEST4-gRNA
BEST4-HA
HA
BEST4
E-cadherin
ZO-1
Vimentin
Twist1
β-actin
E
HCT116-EV
HCT116-BEST4-HA
Tumor size (mm³)
Time（Days）
F
Tumor weight (gram)
HCT116-EV
HCT116-BEST4-HA
G
HCT116-EV
HCT116-BEST4-HA
HA
Ki67
H
Tumour cell proliferation
Positive Ki67 cells (%)
HCT116 -EV
HCT116 -BEST4-HA
I
Mouse
HCT116-EV
HCT116-BEST4-HA
BEST4
E-Cadherin
Vimentin
Twist1
β-actin
J
Relative pixel intensity
HCT116-EV
HCT116-BEST4-HA
BEST4
E-cadherin
Vimentin
Twist1
K
HCT-15
EV-gRNA
BEST4-gRNA
BEST4-Rescued
L
Metastatic tumour number
EV-gRNA
BEST4-gRNA
BEST4-Rescued

Figure 3

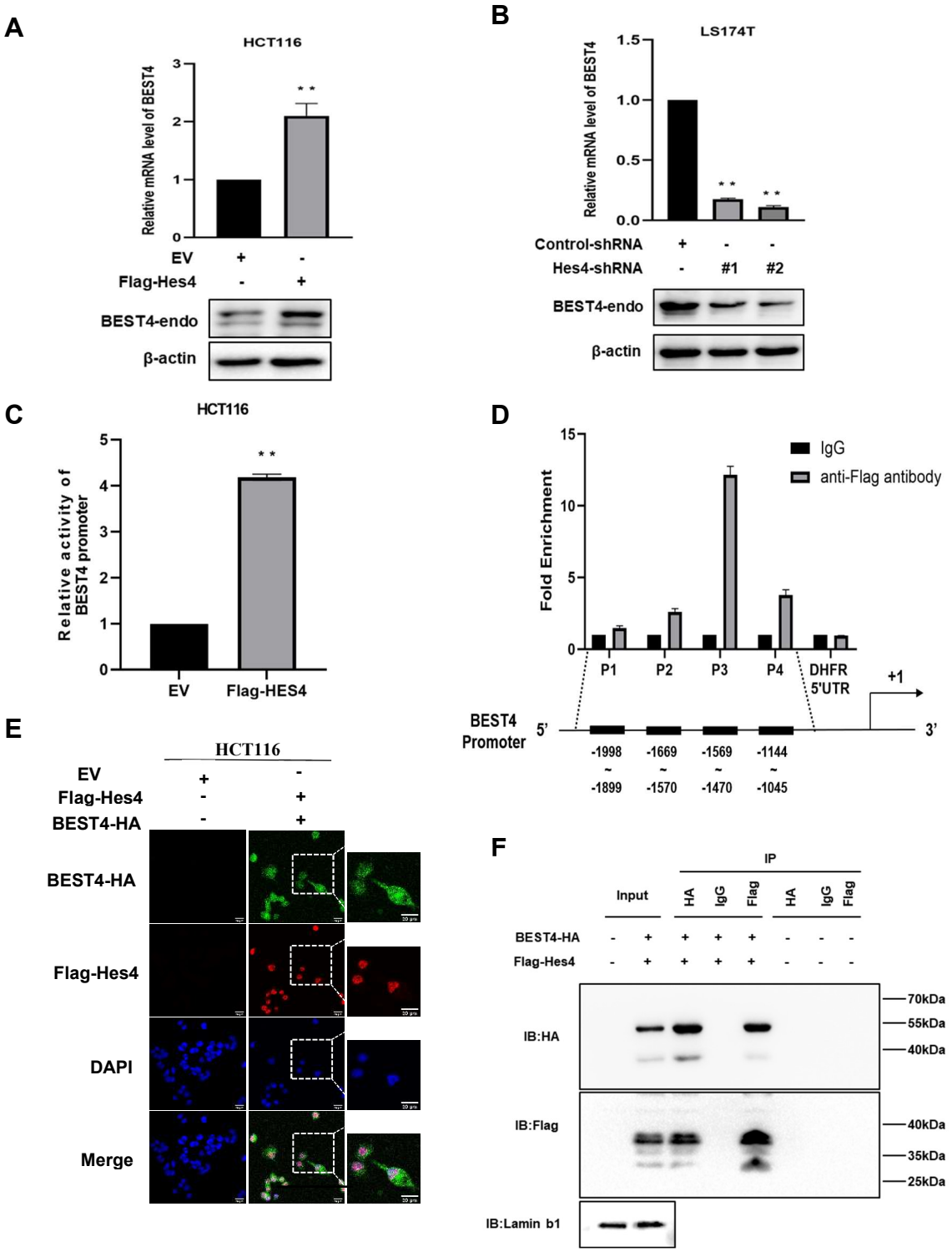
A
HCT116
Relative mRNA level of BEST4
EV
Flag-Hes4
BEST4-endo
β-actin
B
LS174T
Relative mRNA level of BEST4
Control-shRNA
Hes4-shRNA
#1
#2
BEST4-endo
β-actin
C
HCT116
Relative activity of BEST4 promoter
EV
Flag-HES4
D
IgG
anti-Flag antibody
Fold Enrichment
P1
P2
P3
P4
DHFR 5'UTR
+1
BEST4 Promoter
5'
3'
-1998 ~ -1899
-1669 ~ -1570
-1569 ~ -1470
-1144 ~ -1045
E
HCT116
EV
Flag-Hes4
BEST4-HA
BEST4-HA
Flag-Hes4
DAPI
Merge
F
IP
Input
HA
IgG
Flag
BEST4-HA
Flag-Hes4
IB:HA
IB:Flag
IB:Lamin b1
70kDa
55kDa
40kDa
35kDa
25kDa

Figure 4

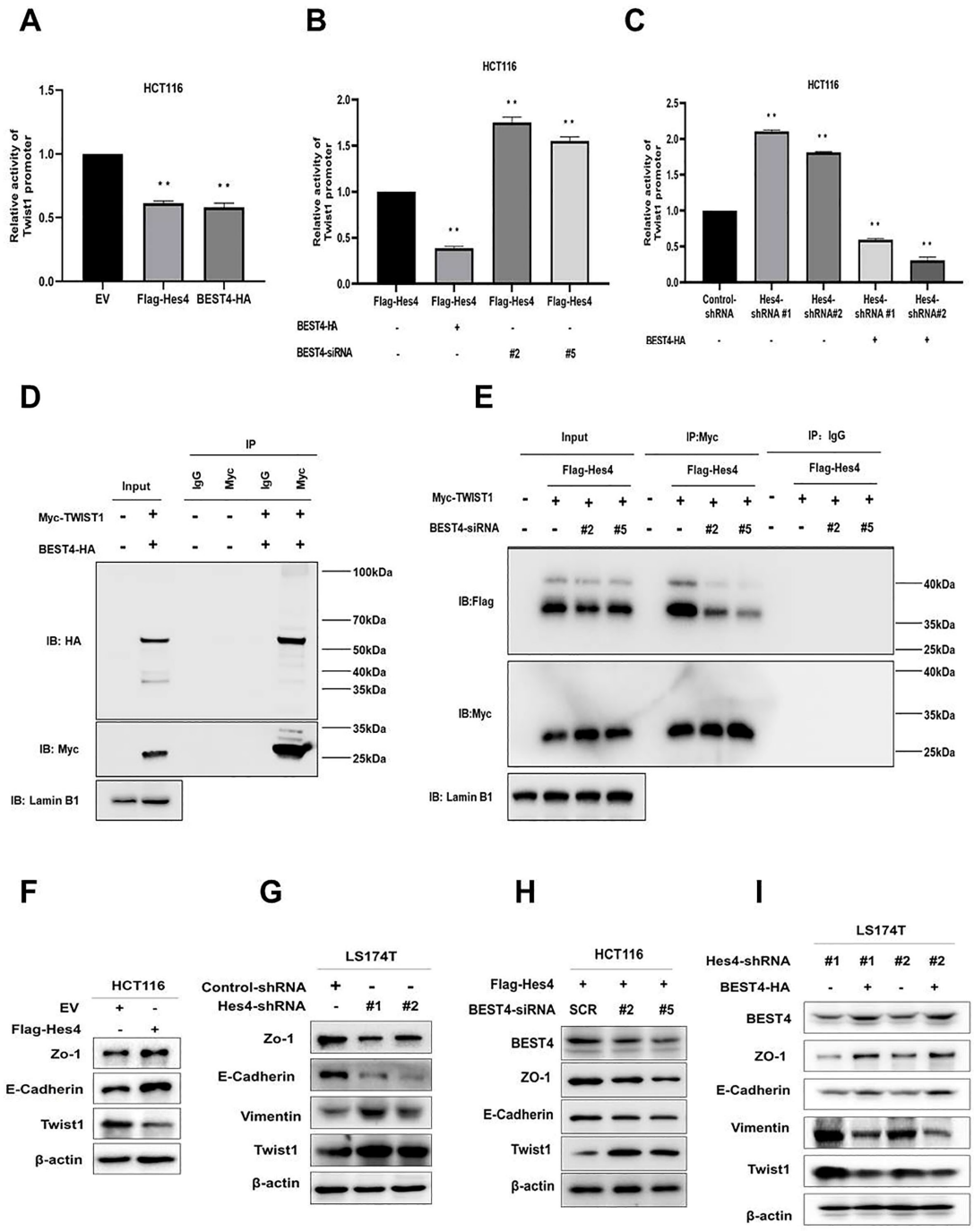
A
HCT116
Relative activity of Twist1 promoter
EV
Flag-Hes4
BEST4-HA
B
HCT116
Relative activity of Twist1 promoter
Flag-Hes4
BEST4-HA
BEST4-siRNA
#2
#5
C
HCT116
Relative activity of Twist1 promoter
Control-shRNA
Hes4-shRNA #1
Hes4-shRNA#2
BEST4-HA
D
IP
Input
IgG
Myc
Myc-TWIST1
BEST4-HA
IB: HA
IB: Myc
IB: Lamin B1
100kDa
70kDa
50kDa
40kDa
35kDa
25kDa
E
Input
IP:Myc
IP: IgG
Flag-Hes4
Myc-TWIST1
BEST4-siRNA
IB:Flag
IB:Myc
IB: Lamin B1
40kDa
35kDa
25kDa
F
HCT116
EV
Flag-Hes4
Zo-1
E-Cadherin
Twist1
β-actin
G
LS174T
Control-shRNA
Hes4-shRNA
#1
#2
Zo-1
E-Cadherin
Vimentin
Twist1
β-actin
H
HCT116
Flag-Hes4
BEST4-siRNA
SCR
#2
#5
BEST4
ZO-1
E-Cadherin
Twist1
β-actin
I
LS174T
Hes4-shRNA
BEST4-HA
BEST4
ZO-1
E-Cadherin
Vimentin
Twist1
β-actin

Figure 5

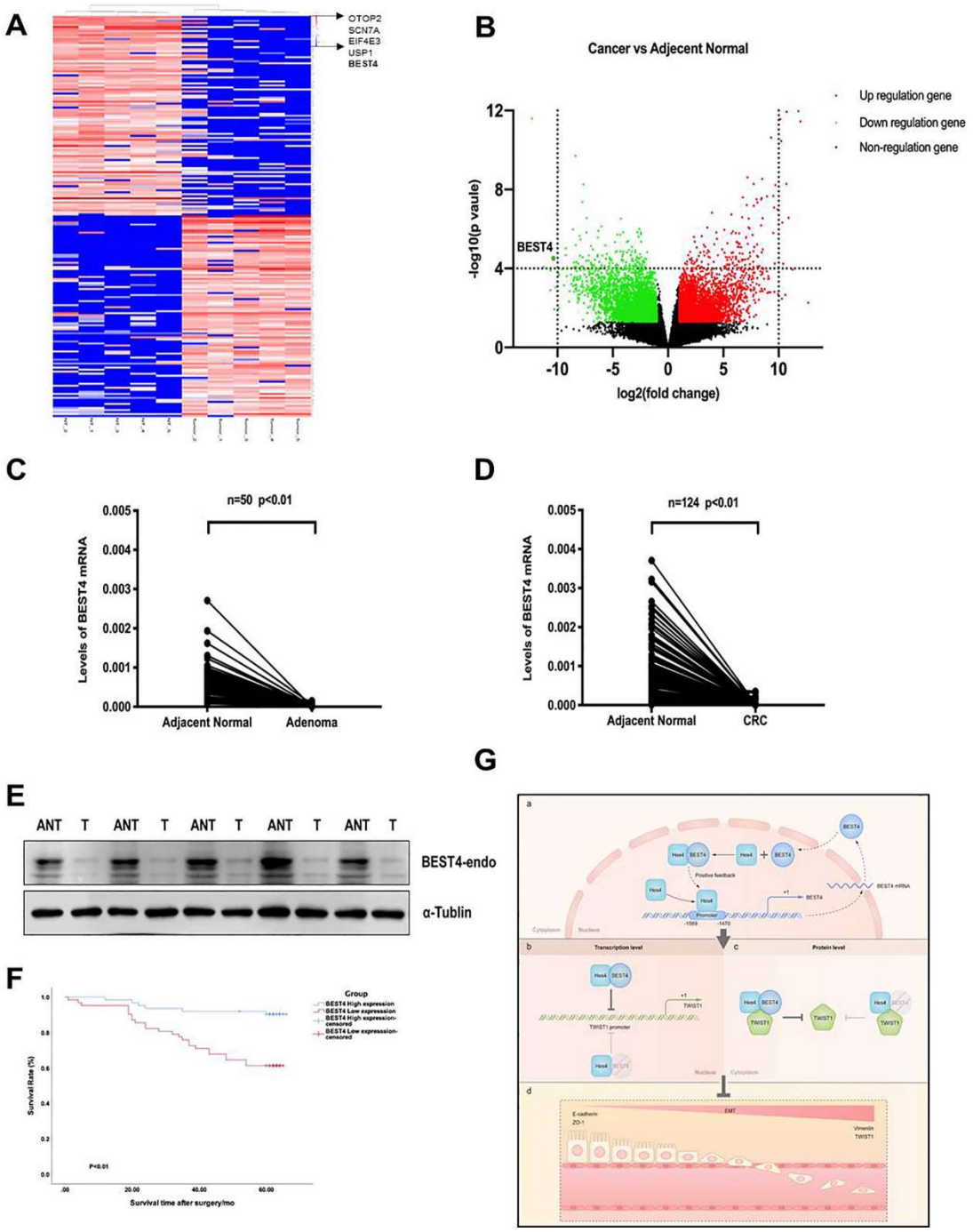
A
OTOP2
SCN7A
EIF4E3
USP1
BEST4
B
Cancer vs Adjecent Normal
Up regulation gene
Down regulation gene
Non-regulation gene
-log10(p vaule)
log2(fold change)
BEST4
C
n=50 p<0.01
Levels of BEST4 mRNA
Adjacent Normal
Adenoma
D
n=124 p<0.01
Levels of BEST4 mRNA
Adjacent Normal
CRC
E
ANT T ANT T ANT T ANT T ANT T
BEST4-endo
α-Tublin
F
Group
Survival Rate (%)
Survival time after surgery/mo
G

937 **Table1. Correlation of *BEST4* mRNA level with clinicopathological factors.**

Parameter	n	*BEST4* expression		P value
		Low	High	
Age (yr)				.66
<60	58	30	28	
≥60	67	32	35	
Sex				**.022***
Male	74	43	31	
Female	51	19	32	
Tumor differentiation				.258
Poor	10	3	7	
Moderate	114	59	55	
Well	1	0	1	
Tumor stage (TNM)[a]				
I	23	10	13	**.02***
II	50	18	32	
III	43	27	16	
IV	9	7	2	
Lymph node metastasis				**.032***
N0	75	30	45	
N1	41	26	15	
N2	9	6	3	
Distant metastasis				.08
Absent	116	55	61	
Present	9	7	2	
Location				.114

Colon	32	12	20	
Rectum	93	50	43	
CEA level				.13
Low	63	27	26	
High	62	35	27	

938 [a] Staging was performed according to the eighth edition of AJCC (M. B. Amin et al.,
939 Springer, 2017)

940 [*] Statistically significant.

941

942

943

944

945

946

947

948

949

950

951

952

953

954 **Table 2. Univariate and Multivariate analysis of prognostic factors for overall**
955 **survival of patients with CRC.**

Variable	Comparison	Univariate analysis, P (log-rank test)	Multivariate analysis		
			HR	95%CI	P
Age (yr)	≥60 vs <60	**.001***	2.713	1.524-4.810	**.001***
Sex	female vs male	.681	NA	NA	NA
Clinical stage	II, III, IV vs I	.1	NA	NA	NA
Tumor differentiation	moderate, well vs poor	.08	NA	NA	NA
Lymph node metastasis	N1, N2 vs N0	**<0.001***	2.190	1.291-3.717	**.004***
Distant metastasis	present vs absent	**<0.001***	2.185	1.103-4.328	**.025***
Location	rectum vs colon	.22	NA	NA	NA
CEA level	high vs low	**.002***	1.697	0.953-2.960	**.073**
BEST4 level	high vs low	**<0.001***	.285	0.157-.606	**<0.001***

956 Abbreviations: HR, hazard ratio; CI, confidence interval; NA, not applicable.
957 * Statistically significant.
958
959
960
961
962

963 **Figure 1-supplemental figure 1.**

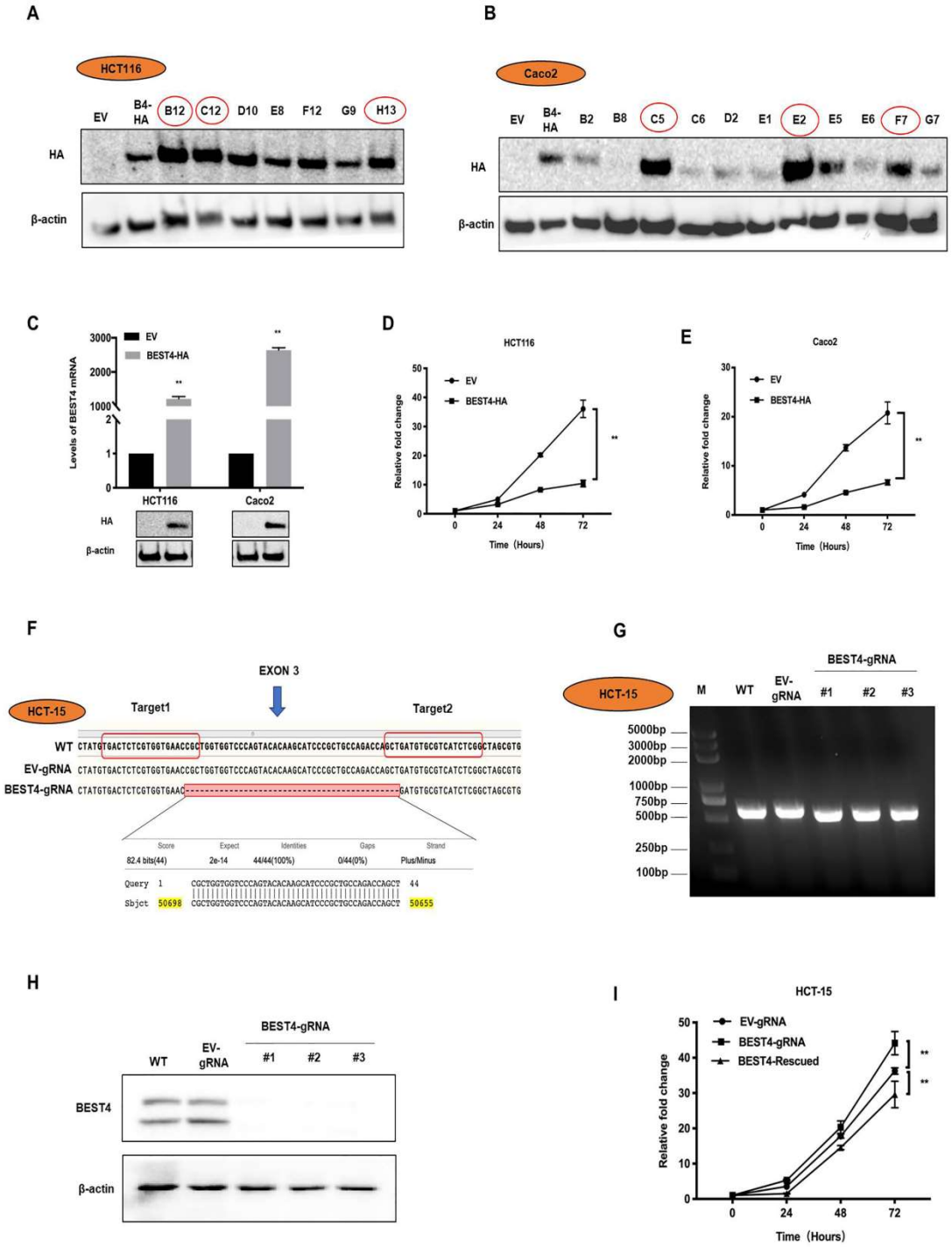

964

965

966

967

968 **Figure 3-supplemental figure 1.**

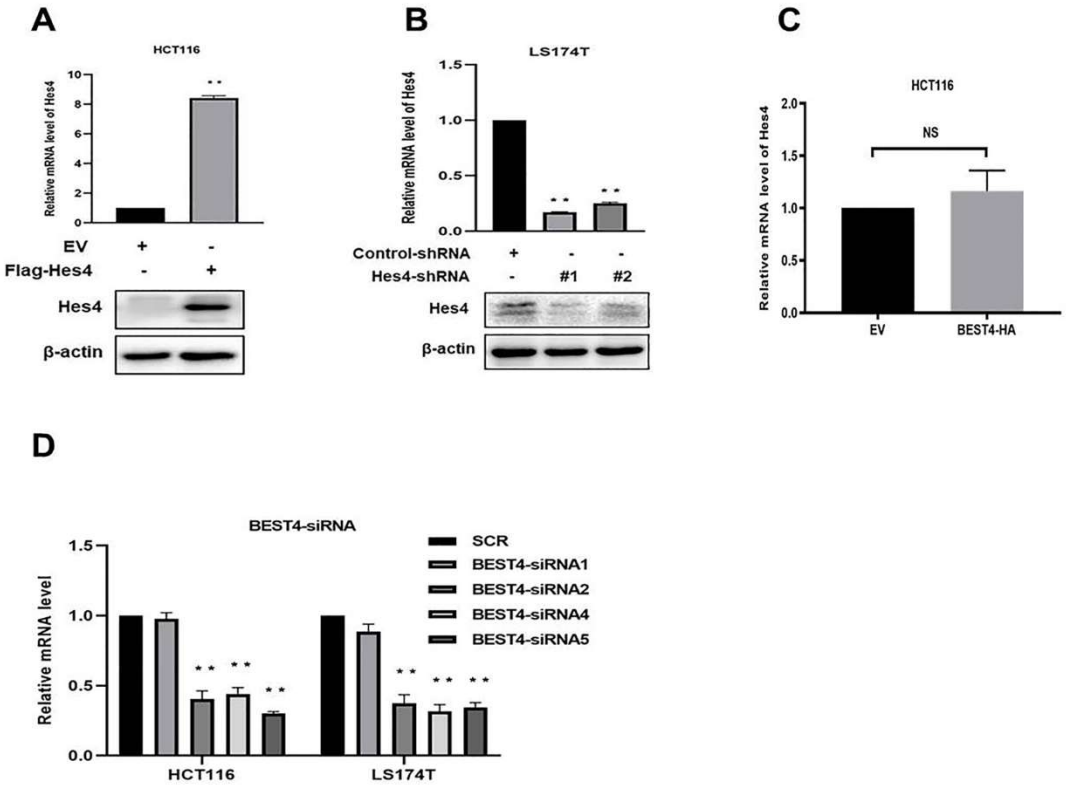

969

970

971

972

973

974

975

976

977

978

979 **Figure 4-supplemental figure 1.**

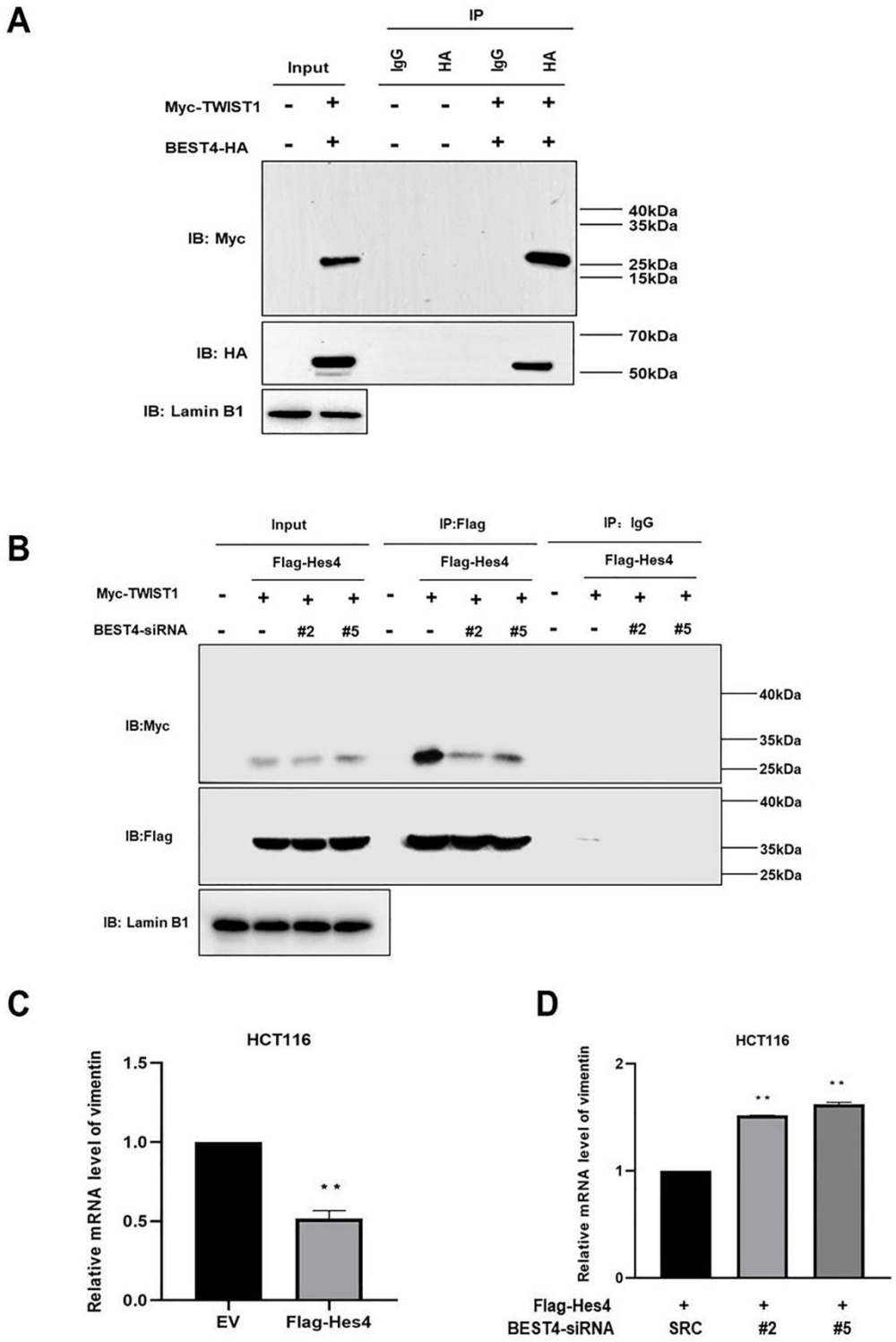

980

981

982

983 **Figure 5-supplemental figure 4**

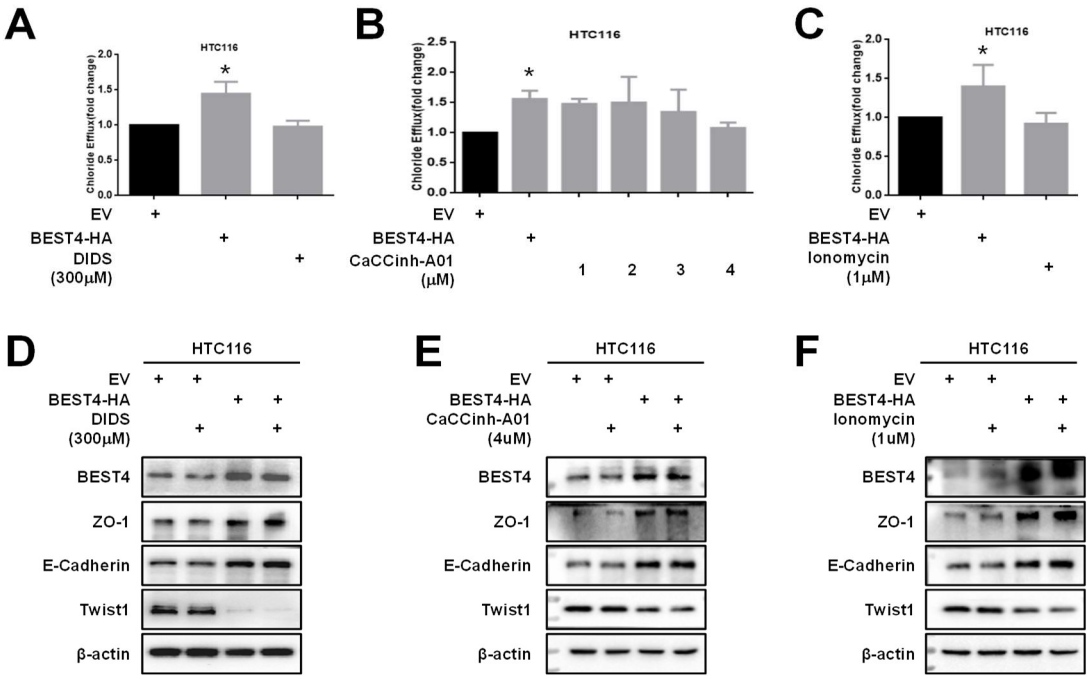

984

985

986

987

988

989

990

991

992

993

994

995

Figure 6-supplemental figure 1.

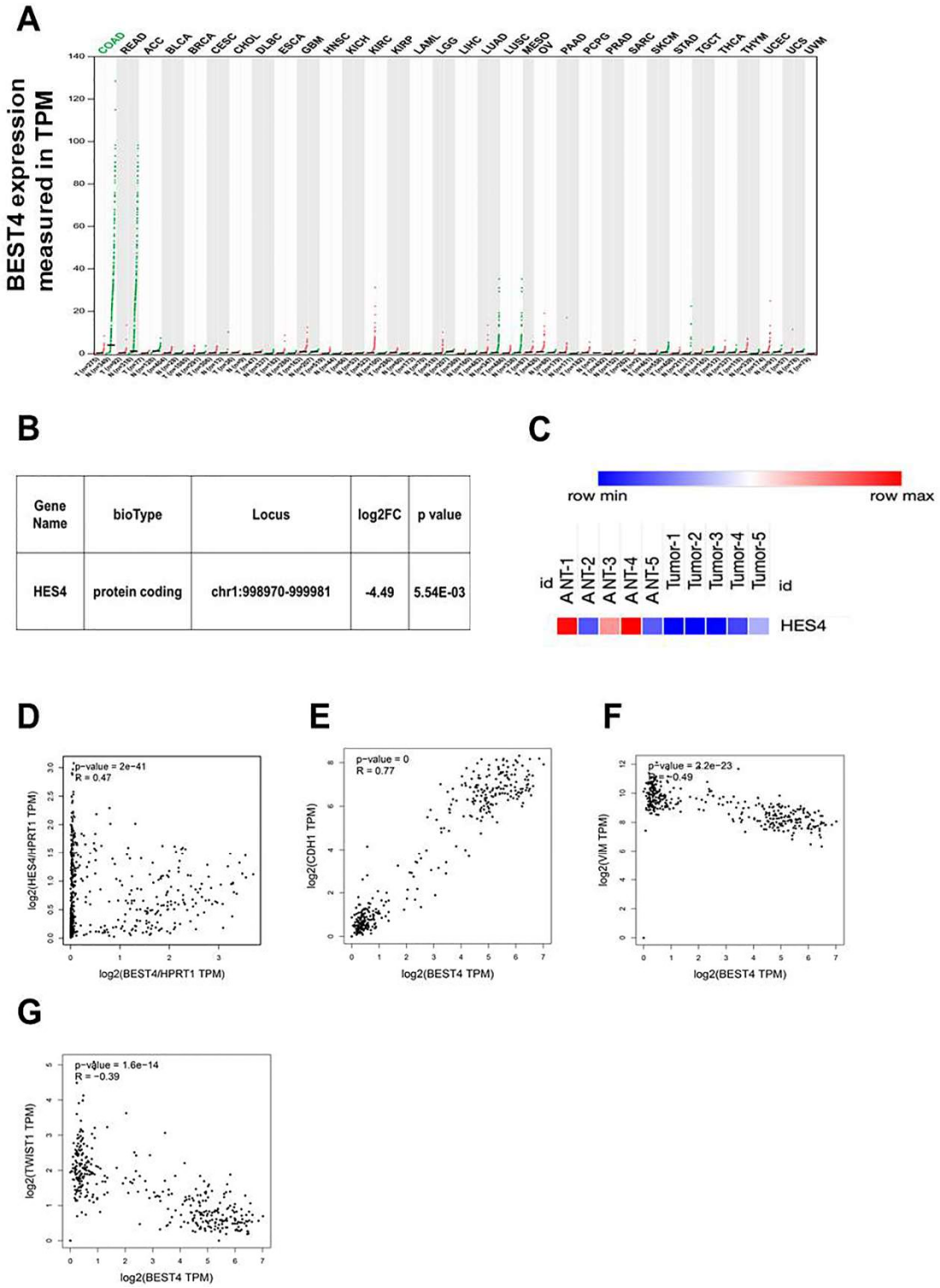

Gene Name	bioType	Locus	log2FC	p value
HES4	protein coding	chr1:998970-999981	-4.49	5.54E-03

999 **Table S1. The target sequence of shRNAs, siRNAs and primers used in this study.**

NAME	5'-3' sequence
Hes4-shRNA 01	5'-CCACGAGTGTCTGGCGGAGGT-3'
Hes4-shRNA 02	5'-ACATCCTGGAGATGACCGTGA-3'
BEST4-siRNA 01	5'-CAAGTGCAGCATGCATTCCA-3'
BEST4-siRNA 02	5'-ATCACGGAAGGTCTTGTCAAA-3'
BEST4-siRNA 04	5'-TACCCTGGTAACCTTACTCAA-3'
BEST4-siRNA 05	5'-ACGGGCGAATACGTGACGATA-3
BEST4	Forward: 5'-CATCACCTACCGGCTG CT-3' Reverse: 5'-GCTGATGTGCGTCATCTCGG-3'
CDH1	Forward: 5'-CATCACCTACCGGCTG CT-3' Reverse: 5'-GCTGATGTGCGTCATCTCGG-3'
Vimentin	Forward: 5'-AACTTCTCAGCATCCGATGAC-3' Reverse: 5'-TTGTAGGAGTGTCGGTTGTTAAG-3'
Zo-1	Forward: 5'-AGGGGCAGTGGTGGTTTTCTGTTCTTTC-3' Reverse: 5'-GCAGAGGTCAAAGTTCAAGGCTCAAGAGG-3'
Twist1	Forward: 5'-AGCTACGCCTTCTCGGTCT-3' Reverse: 5'-CCTTCTCTGGAAACAATGACATC-3'
Hes4	Forward: 5'-GACCCGCAGTCCTCCAA-3' Reverse: 5'-TCCGCCTTCTCCAGCTTC-3'
GAPDH	Forward: 5'-ACTCCTCCACCTTTGACGC-3' Reverse: 5'-GCTGTAGCCAAATTCGTTGTC-3'
P1	Forward: 5'- CTCTCTGTGGCCCAGGCTGGA-3' Reverse: 5'-GCACCAGCTGTAGTCCCAGCT-3'
P2	Forward: 5'-GAGAGGAGTCTCACTCTTT-3' Reverse: 5'-AATGGCGTGAACCTGGGAGG-3'
P3	Forward: 5'-GCCTCCTGAGTAGCTGGGAC-3' Reverse: 5'-TCATGAGGTCAGGAGATCGA-3'
P4	Forward: 5'-GTGATCCCACCTCTGGGCTC -3' Reverse: 5'-CCCTGGCGTGACCTGTCGGT-3'

DHFR	Forward: 5’-CTGATGTCCAGGAGGAGAAAGG-3’
5’ UTR	Reverse: 5’-AGCCCGACAATGTCAAGGACTG-3’

1000

1001